

Distribution of the number of fitness maxima in Fisher's Geometric Model

Su-Chan Park¹, Sungmin Hwang², and Joachim Krug³

¹ Department of Physics, The Catholic University of Korea, Bucheon 14662, Republic of Korea

² Capital Fund Management, 23-25 Rue de l'Université, 75007 Paris, France

³ Institute for Biological Physics, University of Cologne, Zùlpicher Strasse 77, 50937 Köln, Germany

3 December 2021

Abstract. Fisher's geometric model describes biological fitness landscapes by combining a linear map from the discrete space of genotypes to an n -dimensional Euclidean phenotype space with a nonlinear, single-peaked phenotype-fitness map. Genotypes are represented by binary sequences of length L , and the phenotypic effects of mutations at different sites are represented by L random vectors drawn from an isotropic Gaussian distribution. Recent work has shown that the interplay between the genotypic and phenotypic levels gives rise to a range of different landscape topographies that can be characterised by the number of local fitness maxima. Extending our previous study of the mean number of local maxima, here we focus on the distribution of the number of maxima when the limit $L \rightarrow \infty$ is taken at finite n . We identify the typical scale of the number of maxima for general n , and determine the full scaled probability density and two point correlation function of maxima for the one-dimensional case. We also elaborate on the close relation of the model to the anti-ferromagnetic Hopfield model with n random continuous pattern vectors, and show that many of our results carry over to this setting. More generally, we expect that our analysis can help to elucidate the fluctuation structure of metastable states in various spin glass problems.

Submitted to: *J. Phys. A: Math. Theor.*

1. Introduction

The concept of a fitness landscape has proven to be useful in describing the dynamics of evolving biological populations [1, 2, 3]. The fitness landscape is a mapping $W(\sigma)$ that assigns a fitness value to each genetic sequence or *genotype* σ [2, 3, 4, 5]. While natural selection can be conceptualised as a hill-climbing process favouring fitter genotypes, random mutations generate and maintain the genetic diversity that selection acts upon. Equipped with specific rules for the evolutionary dynamics, the changes in genotype frequencies are given by transition rates $\sigma \rightarrow \sigma'$ that typically depend on the fitness

differences $W(\sigma') - W(\sigma)$ between neighbouring genotypes [6, 7, 8]. Thus, determining the functional form of $W(\sigma)$ is a crucial step for modelling the evolution of populations.

Instead of considering a single instance of a fitness function, one often defines random fitness landscape ensembles based on a plausible set of assumptions [5, 9, 10]. By studying the statistical properties of such ensembles, topographical features of typical fitness landscapes corresponding to a given set of assumptions can be inferred. One large class of fitness landscape ensembles are *phenotypic fitness landscapes*. These ensembles introduce an intermediate phenotypic space [11, 12] that mediates the mapping from genotype to fitness through a relation of the form $W(\sigma) = f(\vec{z}(\sigma))$, where $\vec{z}(\sigma)$ is the phenotype and $f(\vec{z})$ the phenotype-fitness map.

Fisher's geometric model (FGM) is the paradigmatic representative of a phenotypic fitness landscape ensemble [13, 14, 15, 16, 17, 18, 19]. Apart from additional model-specific settings, it shares three major ingredients: i) An organism is characterised by a phenotype represented by a vector $\vec{z} = (z_1, z_2, \dots, z_n)$ in an n -dimensional Euclidean space. The real-valued components z_i describe quantitative traits of the organism such as its body mass or size. ii) Mutations in the genotype space induce random displacements $\vec{\xi}$ of phenotypes, by which the population explores the phenotype space. Importantly, the random displacements corresponding to different mutations are added vectorially [14]. iii) A single-peaked fitness function $f(\vec{z})$ forms nonlinear fitness isoclines by which genotype-genotype interactions emerge [17, 20]. The peak of $f(\vec{z})$ defines the location of the optimal phenotype which can be placed at the origin $\vec{z} = 0$ of the trait space without loss of generality.

Having identified these elements, it is not difficult to establish a connection between FGM and disordered discrete spin models. It is based on three observations. First, the presence or absence of a mutation is encoded by a binary variable $\tau_i = \{0, 1\}$, $i = 1, \dots, L$, which can alternatively be represented by an Ising spin $s_i = \{-1, 1\}$. Second, the fitness plays the role of a Hamiltonian of the form $-f(\vec{z}(\sigma))$ and third, the fitness function is determined by the choice of the random displacements $\vec{\xi}$, which introduce quenched disorder into the problem.

In fact, it will be shown below that FGM shares a close similarity with the celebrated Hopfield model of associative memory [21, 22, 23]. In this model, the Hamiltonian is designed such that a set of predefined patterns are the attractors of the corresponding dynamics. Thus, if the initial configuration is closest to one of the stored patterns, it can find it through the dynamics as long as the system is in the retrieval phase. These patterns correspond to the random mutational displacement vectors in FGM, but the interactions turn out to be antiferromagnetic, in the sense that the spin configurations try to avoid predefined patterns. The antiferromagnetic Hopfield model [24] (AFHM) has been studied in various contexts such as the random orthogonal model [25] or minority games [26, 27, 28, 29]. In the present work we will be particularly concerned with the one-dimensional AFHM which is closely related to the number partitioning problem [30, 31].

In our recent contribution [19], we have performed a detailed analysis of the mean

number of local maxima in FGM and determined the phase diagram of the model. Three distinct phases were identified which correspond to different mechanisms by which genotype-genotype interactions and multiple fitness peaks are created. These results were however mostly limited to the mean number of local maxima despite our observation that the number of maxima fluctuates strongly in the limit $L \rightarrow \infty$. Here, we address this issue by computing the higher order moments of the number of maxima. In the case of a one-dimensional phenotype space ($n = 1$) this enables us to determine the full distribution of the number of maxima, which turns out to have a highly nontrivial shape.

In the context of disordered spin systems, the question addressed in this article can be phrased differently: How many metastable states that are stable under single spin flips[‡] exist at zero temperature? This type of question has been studied in various spin glass models using the so-called Tanaka-Edwards formalism [25, 30, 32, 33, 34, 35, 36, 37]. Despite these similarities, an advantage of our model in terms of solvability compared to other spin models relies on the fact that the quantities of interest can be written geometrically. As will be shown below, this feature provides a powerful tool for studying higher-order statistics.

The precise mathematical definition of FGM is provided in the next section. We then discuss the relation to spin models and establish the approximate equivalence with the AFHM in a scaling limit. The calculation of the moments of the number of fitness maxima for general n is explained in section 4, and in section 5 we specialise to the one-dimensional case. In section 6 we derive the pair correlation function of maxima for the one-dimensional model, and conclude in section 7 with a summary and a discussion of the broader context of our work. Detailed derivations are mostly relegated to the appendices.

2. Fisher's geometric model

Following a common convention in population genetics, a genotype is represented by a binary sequence of length L . We denote such a sequence by σ , which sometimes carries an index like σ_α . The binary number appearing at the i th site of the sequence σ is denoted by $\tau_i(\sigma)$ or simply by τ_i if the genotype under consideration is clear from the context. The sequence with $\tau_i = 0$ for all i will be called the wild-type genotype. In biological terms, τ_i represents the presence ($\tau_i = 1$) or absence ($\tau_i = 0$) of a mutation at site i with respect to the wild type.

A phenotype is represented by a vector in the n -dimensional Euclidean trait space \mathbb{R}^n . As a consequence of the assumption of additivity of mutational effects on the

[‡] Note that these states do not necessarily correspond to metastable phases in the thermodynamic sense.

phenotype [14], the phenotype vector \vec{z} corresponding to a genotype σ is constructed as

$$\vec{z}(\sigma) = \vec{Q} + \sum_{i=1}^L \tau_i \vec{\xi}_i, \quad (1)$$

where \vec{Q} is the wild-type phenotype and $\vec{\xi}_i$ describes the change in the phenotype due to a point mutation at site i . The $\vec{\xi}_i$'s are taken to be independent and identically distributed (i.i.d.) random vectors drawn from a common probability density $p(\vec{\xi})$. For convenience we usually choose $p(\vec{\xi})$ as a multivariate Gaussian distribution

$$p(\vec{\xi}) \equiv \frac{1}{(2\pi)^{n/2}} \exp\left(-\frac{1}{2}|\vec{\xi}|^2\right), \quad (2)$$

but most of our results readily generalise to other probability densities that have a finite variance and non-vanishing weight at the origin. In (2) the variance has been set to unity, which implies that distances in the trait space are measured in units of single mutational effects. In particular, $|\vec{Q}|$ is proportional to the minimal number of mutations required to reach the fitness optimum from the wild type.

By composing (1) with a phenotype-fitness map $f(\vec{z})$, we obtain the L -dimensional genotypic fitness landscape

$$W(\sigma) \equiv f(\vec{z}(\sigma)). \quad (3)$$

In the class of models known as FGM the phenotype-fitness function is taken to be single peaked, with the unique phenotypic optimum located at $\vec{z} = 0$. We will also assume isotropy in trait space, which implies that f depends only on $|\vec{z}|$. Different choices for the shape of the fitness peak have been considered in the literature [15], and statistical analyses have been employed to infer the shape function, the dimensionality of trait space, n , and the distance of the wild type to the peak, $|\vec{Q}|$, from experimental data [20, 38, 39].

In this paper, we are interested in how the number \mathcal{N} of local fitness maxima in the genotypic landscape $W(\sigma)$ is distributed for large L . Here, by a local maximum we mean a genotype whose fitness is larger than that of all L neighbours that can be reached by adding ($\tau_i = 0 \rightarrow 1$) or removing ($\tau_i = 1 \rightarrow 0$) a single mutation. Since fitness is a decreasing function of the magnitude of the phenotype vector \vec{z} , the condition that a genotype is a local maximum is purely determined by the ordering of $|\vec{z}|$. Thus, we do not need specify the precise form of the phenotype-fitness map $f(\vec{z})$ for our purposes.

3. Comparison to the antiferromagnetic Hopfield model

3.1. FGM as a spin model

Our problem is identical to counting the number of local *minima* of the quadratic Hamiltonian defined as

$$H_{\text{FGM}} \equiv |\vec{z}(\sigma)|^2 = |\vec{Q} + \sum_i \tau_i \vec{\xi}_i|^2 = |\vec{Q}|^2 + \sum_{ij} \vec{\xi}_i \cdot \vec{\xi}_j \tau_i \tau_j + 2\vec{Q} \cdot \sum_i \tau_i \vec{\xi}_i. \quad (4)$$

Minimizing the last (linear) term simply amounts to setting $\tau_i = 1$ ($\tau_i = 0$) whenever $\vec{Q} \cdot \vec{\xi}_i < 0$ ($\vec{Q} \cdot \vec{\xi}_i > 0$). For large $|\vec{Q}|$ this term dominates and the fitness landscape becomes approximately additive [19].

To elucidate the meaning of the quadratic term we set $\vec{Q} = 0$ and rewrite (4) in terms of the Ising spins $s_i \equiv 2\tau_i - 1$. This yields

$$H_{\text{FGM}}^{\vec{Q}=0} = \frac{1}{4} \sum_{ij} J_{ij} s_i s_j + \frac{1}{2} \sum_i \tilde{h}_i s_i + \frac{1}{4} \sum_{ij} J_{ij}, \quad (5)$$

where

$$J_{ij} \equiv \sum_{k=1}^n \xi_i^k \xi_j^k, \quad \tilde{h}_i = \sum_{k=1}^n \left(\sum_{j=1}^L \xi_j^k \right) \xi_i^k, \quad (6)$$

and ξ_i^k is the k th component of $\vec{\xi}_i$. Since the last term in the Hamiltonian is a global constant for a given realization of $\vec{\xi}_i$'s, we can remove it without affecting the structure of the energy landscape. Up to a conventional scale factor $\frac{1}{L}$, the interaction term in (5) is identical to the Hamiltonian of the antiferromagnetic Hopfield model

$$H_{\text{AFHM}} = \frac{1}{4L} \sum_{ij} J_{ij} s_i s_j = \frac{1}{4L} \sum_{k=1}^n \left(\sum_{i=1}^L \xi_i^k s_i \right)^2 \quad (7)$$

with n real-valued pattern vectors $(\xi_1^k, \xi_2^k, \dots, \xi_L^k) \in \mathbb{R}^L$. The AFHM Hamiltonian is minimised by spin configurations that are maximally orthogonal to the patterns [24].

The FGM Hamiltonian differs from the AFHM by the presence of the random fields \tilde{h}_i which are determined by the pattern vectors through (6). As a consequence the fields are correlated with the couplings J_{ij} . Although we will argue in the next subsection that these correlated random fields become negligible at least in certain limits, they enforce two fundamental differences between the two models. First, the random fields break the $s_i \rightarrow -s_i$ Ising symmetry of H_{AFHM} . This symmetry implies in particular that the number of local energy minima \mathcal{N} has to be even for the AFHM, while no such constraint applies for FGM. Second, the correlations between the fields and the couplings ensure that the ground state value $H_{\text{FGM}}^{\vec{Q}=0} = 0$ is realised by $s_i \equiv -1$ ($\tau_i = 0$), as is evident from the construction of the model. By contrast, the ground state of H_{AFHM} is nontrivial and generally unknown.

3.2. Joint limit $L, n \rightarrow \infty$

Under the Gaussian distribution (2) for the displacement vectors the interior sum in the definition of the \tilde{h}_i in (6) can be written as

$$\sum_{j=1}^L \xi_j^k = \sqrt{L} \eta_k, \quad (8)$$

where the η_k 's are i.i.d. Gaussian random variables with unit variance. Moreover, since

$$\langle \eta_k \xi_i^k \rangle = \frac{1}{\sqrt{L}} \langle (\xi_i^k)^2 \rangle = \frac{1}{\sqrt{L}}, \quad \langle (\eta_k \xi_i^k)^2 \rangle = 1 + \mathcal{O}(L^{-1}), \quad (9)$$

we can apply the central limit theorem to obtain

$$\tilde{h}_i = \sqrt{L} \sum_{k=1}^n \eta_k \xi_i^k \approx \sqrt{Ln} h_i, \quad (10)$$

where the h_i are i.i.d. Gaussian random variables with zero mean and unit variance that become approximately independent of the ξ_j^k in the joint limit $L, n \rightarrow \infty$.

Specifically, if we take the limit $L \rightarrow \infty$ with $\alpha = n/L$ fixed, the FGM Hamiltonian formally maps to the AFHM with random fields of strength $\sqrt{\alpha}$,

$$\frac{1}{L} H_{\text{FGM}}^{\vec{Q}=0} \approx \frac{1}{4L} \sum_{ij} J_{ij} s_i s_j + \frac{1}{2} \sqrt{\alpha} \sum_i h_i s_i. \quad (11)$$

The correlations between the couplings J_{ij} and the random fields h_i in (11) can be estimated using Wick's theorem, which yields

$$\frac{1}{L} \langle J_{ij} h_p \rangle \approx \frac{1}{L\sqrt{Ln}} \left\langle \sum_k \xi_i^k \xi_j^k \sum_{l=1}^n \sum_{q=1}^L \xi_p^l \xi_q^l \right\rangle \sim \begin{cases} O(\alpha) & i = j \\ O\left(\frac{1}{L}\right) & i = p \text{ or } j = p. \end{cases} \quad (12)$$

This suggests that FGM and the AFHM without random fields should behave similarly at least when α is small. A precise comparison can be made on the level of the exponential growth rate of the expected number of fitness peaks $\langle \mathcal{N} \rangle$ defined by [19]

$$\Sigma^* = \lim_{L \rightarrow \infty} \frac{\ln \langle \mathcal{N} \rangle}{L}. \quad (13)$$

In Appendix A we compute Σ^* for FGM, which behaves as

$$\Sigma_{\text{FGM}}^* \simeq \ln 2 - \frac{\alpha}{2} \ln \left(-\frac{4 \ln \alpha}{e\alpha} \right) = \ln 2 - \frac{\alpha}{2} \ln \left(\frac{|\ln \alpha|}{\alpha} \right) - \frac{\alpha}{2} \ln \left(\frac{4}{e} \right) \quad (14)$$

for $\alpha \rightarrow 0$. This should be compared with the result for the AFHM without random fields given by [25]§

$$\Sigma_{\text{AFH}}^* \simeq \ln 2 - \frac{\alpha}{2} \ln \left(-\frac{2 \ln \alpha}{e\alpha} \right). \quad (15)$$

The two expressions are seen to agree in the leading nontrivial behaviour, which shows that the correlated random fields in (11) contribute only at the subleading order $O(\alpha)$.

In the following sections we focus on the case of finite n , with particular emphasis on the one-dimensional model.

4. Moments

The number \mathcal{N} of local fitness maxima in the genotypic landscape can be formally written as

$$\mathcal{N} = \sum_{\sigma} \mathfrak{I}(\sigma), \quad (16)$$

§ In [25], α' is used in place of α .

where $\mathfrak{J}(\sigma)$ is an indicator that takes the value 1 if σ is a local maximum and 0 otherwise. We begin by writing a formal expression for the m th moment

$$\langle \mathcal{N}^m \rangle = \sum_{\sigma_1, \dots, \sigma_m} \left\langle \prod_{\alpha=1}^m \mathfrak{J}(\sigma_\alpha) \right\rangle, \quad (17)$$

where $\langle \dots \rangle$ stands for the average over the ensemble of $\vec{\xi}_i$'s. Since $\langle \mathfrak{J}(\sigma_1) \mathfrak{J}(\sigma_2) \dots \mathfrak{J}(\sigma_m) \rangle$ is simply the joint probability $P_m(\sigma_1, \sigma_2, \dots, \sigma_m)$ that the indicated genotypes are local maxima, we can rewrite the m th moment as

$$\langle \mathcal{N}^m \rangle = \sum_{\sigma_1, \dots, \sigma_m} P_m(\sigma_1, \dots, \sigma_m). \quad (18)$$

For a genotype σ_α to be a local maximum, every $\vec{\xi}_i$ has to satisfy the condition [19]

$$\left| \vec{z}_\alpha + (1 - 2\tau_i) \vec{\xi}_i \right| > |\vec{z}_\alpha|, \quad (19)$$

where $\vec{z}_\alpha = \vec{z}(\sigma_\alpha)$ is the phenotype associated with genotype σ_α . Defining the domain

$$\mathcal{D}[\vec{z}] = \{ \vec{y} \in \mathbb{R}^n \mid |\vec{y} - \vec{z}| > |\vec{z}| \}, \quad (20)$$

we can succinctly write the condition for m genotypes to be simultaneous local maxima as

$$\vec{\xi}_i \in \mathcal{A}_i \equiv \bigcap_{\alpha=1}^m \mathcal{D}[(2\tau_{i,\alpha} - 1) \vec{z}_\alpha], \quad (21)$$

where $\tau_{i,\alpha} \equiv \tau_i(\sigma_\alpha)$. Using the definition of phenotype vectors (1), we get

$$\begin{aligned} P_m &= \int_{\mathbb{R}^n} \left(\prod_{\alpha=1}^m d\vec{z}_\alpha \right) \left[\prod_{j=1}^L \int_{\mathcal{A}_j} d\vec{\xi}_j p(\vec{\xi}_j) \right] \prod_{\alpha=1}^m \delta \left(\vec{z}_\alpha - \vec{Q} - \sum_{l=1}^L \vec{\xi}_l \tau_{l,\alpha} \right) \\ &= \int_{\mathbb{R}^n} \prod_{\alpha=1}^m \frac{d\vec{z}_\alpha d\vec{k}_\alpha}{(2\pi)^n} \exp \left(i\vec{k}_\alpha \cdot (\vec{z}_\alpha - \vec{Q}) \right) \left[\prod_{j=1}^L \int_{\mathcal{A}_j} d\vec{\xi}_j p(\vec{\xi}_j) \exp \left(-i\vec{\xi}_j \cdot \sum_{\beta=1}^m \vec{k}_\beta \tau_{j,\beta} \right) \right], \quad (22) \end{aligned}$$

where the Fourier representation of the delta function is used and the arguments of P_m are omitted for brevity.

Now we are ready to find a formal expression for the m th moment. Using that

$$\begin{aligned} & \sum_{\sigma_1, \dots, \sigma_m} \prod_j \int_{\mathcal{A}_j} d\vec{\xi}_j p(\vec{\xi}_j) \exp \left(-i\vec{\xi}_j \cdot \sum_{\beta=1}^m \vec{k}_\beta \tau_{j,\beta} \right) \\ &= \prod_{j=1}^L \left[\sum_{\tau_{j,1}=0}^1 \dots \sum_{\tau_{j,m}=0}^1 \int_{\mathcal{A}_j} d\vec{\xi}_j p(\vec{\xi}_j) \exp \left(-i\vec{\xi}_j \cdot \sum_{\beta=1}^m \vec{k}_\beta \tau_{j,\beta} \right) \right], \quad (23) \end{aligned}$$

we arrive at

$$\langle \mathcal{N}^m \rangle = \int_{\mathbb{R}^n} \prod_{\alpha=1}^m \frac{d\vec{z}_\alpha d\vec{k}_\alpha}{(2\pi)^n} \exp \left(i\vec{k}_\alpha \cdot (\vec{z}_\alpha - \vec{Q}) \right) (S_m)^L, \quad (24)$$

where

$$S_m \equiv \sum_{a_1=0}^1 \cdots \sum_{a_m=0}^1 \int_{\mathcal{A}(a)} d\vec{\xi} p(\vec{\xi}) \exp \left(-i\vec{\xi} \cdot \sum_{\beta=1}^m \vec{k}_\beta a_\beta \right), \quad (25)$$

with the domain of integration

$$\mathcal{A}(a) \equiv \bigcap_{\alpha=1}^m \mathcal{D}[(2a_\alpha - 1)\vec{z}_\alpha]. \quad (26)$$

In Appendix B, we calculate S_m and find that for large L

$$\langle \mathcal{N}^m \rangle \approx \mu_m \left(\frac{2^L}{L^{1+n/2}} \right)^m \exp \left(-\frac{2m}{m+1} |\vec{q}|^2 L^{2\gamma-1} \right), \quad (27)$$

where μ_m is a constant independent of L (see (B.11) for the definition). Within this derivation, the scaling of the wild-type phenotype was chosen to be of the form $\vec{Q} = \vec{q}L^\gamma$ with $0 \leq \gamma < 1$, which implies that $q = |\vec{q}|$ can be treated perturbatively in the limit $L \rightarrow \infty$. This approach is no longer valid if $\gamma = 1$ and a separate analysis is required to determine $\langle \mathcal{N}^m \rangle$. In [19], the nontrivial behaviour of $\langle \mathcal{N} \rangle$ for $\gamma = 1$ is discussed in detail.

In the following we consider the case $q = 0$. The fact that $\langle \mathcal{N}^m \rangle$ is proportional to $\left(\frac{2^L}{L^{1+n/2}} \right)^m$ suggests that the rescaled random variable

$$X = \frac{L^{1+n/2}}{2^L} \mathcal{N} \quad (28)$$

attains a nondegenerate limit distribution when $L \rightarrow \infty$. This distribution will be explicitly computed for $n = 1$ in the next section. For general n , the scaling (28) implies that

$$\lim_{L \rightarrow \infty} \frac{\ln \mathcal{N}}{L} = \ln 2 \quad (29)$$

on the level of single realizations. This shows that the exponential growth rate defined in (13) is $\Sigma^* = \ln 2$ in agreement with the $\alpha \rightarrow 0$ limit of (14), and moreover $\ln \mathcal{N}$ becomes a deterministic (self-averaging) quantity for $L \rightarrow \infty$.

The calculation presented in this section carries over in a very similar form to the local energy minima of the AFHM defined by the Hamiltonian (7) (see Appendix I). The same scaling (28) obtained for FGM applies, and the asymptotic expression for the moments given in (I.10) differs from (27) with $q = 0$ by a factor $(m+1)^{n/2}$.

5. Exact distribution in one-dimensional phenotype space

In this section we limit ourselves to the one dimensional case with $q = 0$ and derive the probability density of the rescaled number of fitness maxima in the large L limit. Due to the simple geometry of one-dimensional Euclidean space, it is possible to determine the exact form of the moments μ_m for $n = 1$, from which the full distribution can be extracted.

5.1. Probability density

In Appendix C, the μ_m for $n = 1$ are obtained as

$$\mu_m = \frac{m!Q_m}{\sqrt{m+1}}, \quad Q_m \equiv \left[\left(\frac{1}{2}; \frac{1}{2} \right)_m \right]^{-1}, \quad (30)$$

where we use the q -Pochhammer symbol defined by

$$(a; q)_m \equiv \prod_{k=0}^{m-1} (1 - aq^k), \quad (31)$$

with $(a; q)_0 \equiv 1$. Some properties of the q -Pochhammer symbol are summarised in Appendix D. The μ_m are the moments of the rescaled random variable

$$X = \frac{L^{3/2}}{2^L} \mathcal{N} \quad (32)$$

defined in (28) for general n , and we seek to derive the probability density $P(x)$ of X .

We first consider the moment generating function $\mathcal{G}(k)$ of X and its infinite series representation

$$\mathcal{G}(k) \equiv \int_{-\infty}^{\infty} P(x) \exp(ikx) dx = \sum_{m=0}^{\infty} \frac{\mu_m}{m!} (ik)^m = \sum_{m=0}^{\infty} \frac{Q_m (ik)^m}{\sqrt{m+1}}, \quad (33)$$

where we use (30). Because the radius of convergence of the infinite series is 1, we need an analytic continuation to find the probability density $P(x)$.

As we will see, $\mathcal{G}(k)$ can be written in terms of the Lerch transcendent defined as [40]

$$\Phi(z, s, v) \equiv \sum_{m=0}^{\infty} \frac{z^m}{(m+v)^s}. \quad (34)$$

Although Φ is defined for complex s and v , we are only interested in the case where $v = 1$ and s is real throughout this article. The third argument of Φ will therefore be dropped in what follows. The analytic continuation is obtained using the integral representation of $\Phi(z, s)$ [40]

$$\Phi(z, s) = \frac{1}{\Gamma(s)} \int_0^{\infty} \frac{t^{s-1}}{e^t - z} dt. \quad (35)$$

If a branch cut is made from $z = 1$ to $z = \infty$ along the real z axis, $\Phi(z, s)$ is an analytic function in the cut plane for $s > 0$.

Using (D.4) and (34), we rewrite $\mathcal{G}(k)$ as

$$\begin{aligned} \mathcal{G}(k) &= S \sum_{m=0}^{\infty} \frac{(ik)^m}{\sqrt{m+1}} \sum_{l=0}^{\infty} \frac{2^{-lm}}{(2; 2)_l} \\ &= S \sum_{l=0}^{\infty} \frac{1}{(2; 2)_l} \sum_{m=0}^{\infty} \frac{(ik2^{-l})^m}{\sqrt{m+1}} = S \sum_{l=0}^{\infty} \frac{\Phi(ik2^{-l}, \frac{1}{2})}{(2; 2)_l}, \end{aligned} \quad (36)$$

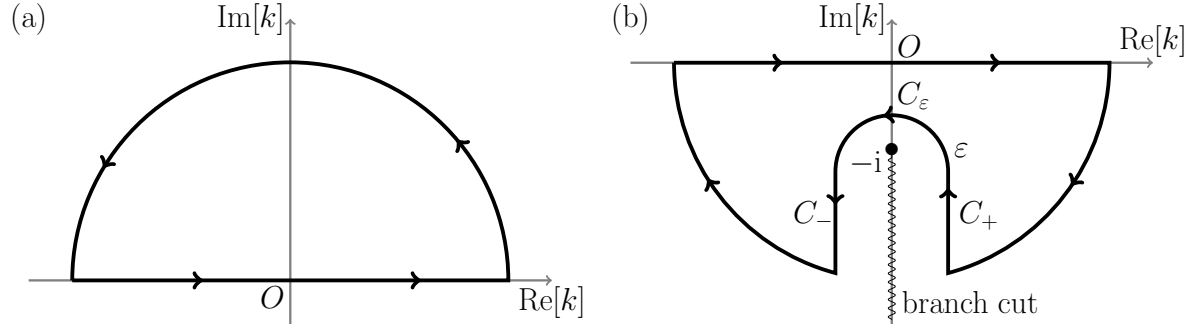


Figure 1. Contour for the integral (39). (a) Contour for negative y . (b) Contour for positive y . The branch point $-i$ is indicated by a solid circle (\bullet) and the branch cut is indicated by a wiggly line. C_+ is the contour from $\varepsilon - i\infty$ to $\varepsilon - i$ and C_- is that from $-\varepsilon - i$ to $-\varepsilon - i\infty$. The limit $\varepsilon \rightarrow 0$ is performed at the end of the calculation.

where

$$S \equiv \left[\left(\frac{1}{2}; \frac{1}{2} \right)_{\infty} \right]^{-1} \approx 3.4627466. \quad (37)$$

Thus, we found a continuation of $\mathcal{G}(k)$ that is analytic in a Riemann sheet with a branch cut $ik > 1$.

Next, the probability density is obtained by the inverse Fourier transformation

$$\begin{aligned} P(x) &= \frac{1}{2\pi} \int_{-\infty}^{\infty} \exp(-ikx) \mathcal{G}(k) dk \\ &= \frac{S}{2\pi} \sum_{l=0}^{\infty} \frac{1}{(2; 2)_l} \int_{-\infty}^{\infty} \exp(-ikx) \Phi\left(ik2^{-l}, \frac{1}{2}\right) dk = S \sum_{l=0}^{\infty} \frac{2^l}{(2; 2)_l} \psi(2^l x), \end{aligned} \quad (38)$$

where

$$\psi(y) \equiv \frac{1}{2\pi} \int_{-\infty}^{\infty} \exp(-iky) \Phi\left(ik, \frac{1}{2}\right) dk. \quad (39)$$

For $y < 0$, we consider the contour in the complex k plane shown in figure 1 (a). Since $\Phi(ik)$ has a branch point at $ik = 1$ and a branch cut $ik > 1$ [see figure 1 (b)], the contour integral gives $\psi(y) = 0$. Thus, $P(x) = 0$ for $x < 0$ as it should be.

For positive y , we consider the contour in figure 1 (b). Since $\Phi(z, \frac{1}{2}) \sim 1/\sqrt{1-z}$ for $|1-z| \ll 1$ [40], the integral over C_ε approaches zero as $\varepsilon \rightarrow 0$. Hence, the nonzero contribution to the integral comes from the contours C_+ and C_- :

$$\begin{aligned} \psi(y) &= -\frac{1}{2\pi} \lim_{\varepsilon \rightarrow 0} \left[\int_{C_+} + \int_{C_-} \right] \exp(-izy) \Phi\left(iz, \frac{1}{2}\right) dz \\ &= \frac{1}{2\pi i} \lim_{\varepsilon \rightarrow 0} \int_1^{\infty} e^{-yw} \left[e^{-i\varepsilon y} \Phi\left(w + i\varepsilon, \frac{1}{2}\right) - e^{i\varepsilon y} \Phi\left(w - i\varepsilon, \frac{1}{2}\right) \right] dw \\ &= \frac{1}{\pi} \lim_{\varepsilon \rightarrow 0} \int_1^{\infty} e^{-yw} \Im \Phi\left(w + i\varepsilon, \frac{1}{2}\right) dw, \end{aligned} \quad (40)$$

where $\Im z$ stands for the imaginary part of z and we have used $\Phi(z, s)^* = \Phi(z^*, s)$ (the

asterisk represents complex conjugation). Using

$$\lim_{\varepsilon \rightarrow 0} \frac{1}{x - i\varepsilon} = \frac{1}{x} + i\pi\delta(x), \quad (41)$$

we obtain

$$\Im\Phi\left(w + i\varepsilon, \frac{1}{2}\right) = \Im \int_0^\infty \frac{dt}{\sqrt{\pi t}(e^t - w - i\varepsilon)} = \frac{\sqrt{\pi}}{w\sqrt{\ln w}}, \quad (42)$$

which gives

$$\psi(y) = \frac{1}{\sqrt{\pi}} \int_1^\infty \frac{\exp(-yw)}{w\sqrt{\ln w}} dw = \int_0^\infty \frac{\exp(-ye^t)}{\sqrt{\pi t}} dt. \quad (43)$$

In Appendix E, we derive the same distribution using a slightly different method.

In figure 2, we depict $P(x)$ obtained by numerical evaluation of (43) and (38). One may observe that $P(x)$ seems to approach a nonzero value as $x \rightarrow 0$. A careful analysis presented in Appendix F shows, however, that $P(x) \rightarrow 0$ as $x \rightarrow 0$ with an infinite slope. For large x , $P(x)$ is dominated by the leading order $l = 0$ term in (38) and the asymptotics reflect that of $\psi(x)$. Taken together, the behaviour of $P(x)$ for large and small x is found to be

$$P(x) \sim \begin{cases} \frac{\ln 2}{\sqrt{-\pi \ln x}}, & \text{for } x \ll 1, \\ S \frac{e^{-x}}{\sqrt{x}}, & \text{for } x \gg 1. \end{cases} \quad (44)$$

The asymptotic behavior is compared to the exact probability density in the inset of figure 2.

5.2. Finite L correction

To facilitate the comparison to numerical simulations, we consider the finite- L corrections to the distribution $P(x)$. In Appendix G we obtain the $O(1/L)$ correction to the moments of the rescaled variable X as

$$\frac{\langle X^m \rangle - \mu_m}{m!} = -\frac{3}{4L} \frac{m^2(m+2)Q_m}{(m+1)^{3/2}} + O(L^{-2}). \quad (45)$$

Writing the moment generating function of X for finite L as $\mathcal{G}(k) + \Delta\mathcal{G}(k)$, we get

$$\begin{aligned} -\frac{4L}{3}\Delta\mathcal{G} &\approx \sum_{m=0}^{\infty} \frac{m^2(m+2)}{(m+1)^{3/2}} Q_m (ik)^m \\ &= \sum_{l=1}^{\infty} Q_{l-1} (l^{3/2} - l^{1/2} - l^{-1/2} + l^{-3/2}) (ik)^{l-1} \\ &\equiv \mathcal{G}_{3/2} - \mathcal{G}_{1/2} - \mathcal{G}_{-1/2} + \mathcal{G}_{-3/2}, \end{aligned} \quad (46)$$

where

$$\mathcal{G}_s(k) = \sum_{l=1}^{\infty} Q_{l-1} (ik)^{l-1} l^{-s} = S \sum_{m=0}^{\infty} \frac{\Phi(ik2^{-m}, s)}{(2; 2)_m}. \quad (47)$$

Note that $\mathcal{G}_{1/2}(k) = \mathcal{G}(k)$.

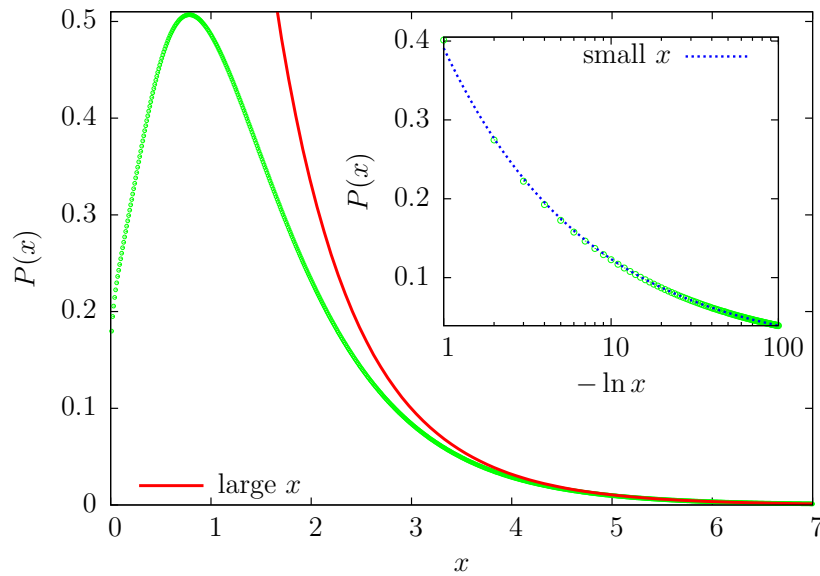


Figure 2. Plot of the probability density $P(x)$ of the scaled number of fitness maxima for FGM with $n = 1$ (green open circles). For comparison, the leading asymptotic behaviour (44) for large x is drawn as a red curve. Inset: semi-logarithmic plot of $P(x)$ vs. $-\ln x$ illustrating the behaviour (44) for small x . A curve showing the leading asymptotics is drawn for comparison (dotted blue line).

If we denote the Fourier transform of $\Phi(ik, s)$ by

$$\psi_s(x) \equiv \frac{1}{2\pi} \int_{-\infty}^{\infty} \exp(-ikx) \Phi(ik, s) dk, \quad (48)$$

we obtain a recursion relation

$$\begin{aligned} \psi_{l-1}(x) &= \frac{1}{2\pi} \int_{-\infty}^{\infty} \exp(-ikx) \Phi(ik, l-1) dk \\ &= \frac{1}{2\pi} \int_{-\infty}^{\infty} \exp(-ikx) \frac{d}{dk} [k\Phi(ik, l)] dk = \left(-x \frac{d}{dx}\right) \psi_l(x), \end{aligned} \quad (49)$$

where we have used

$$\Phi(z, l-1) = \frac{d}{dz} [z\Phi(z, l)]. \quad (50)$$

Since $\psi_{1/2}(x) = \psi(x)$ in (43), we have

$$\begin{aligned} \psi_{-1/2}(x) &= \frac{x}{\sqrt{\pi}} \int_0^{\infty} \frac{\exp(t - xe^t)}{\sqrt{t}} dt, \\ \psi_{-3/2}(x) &= -\psi_{-1/2}(x) + \frac{x^2}{\sqrt{\pi}} \int_0^{\infty} \frac{\exp(2t - xe^t)}{\sqrt{t}} dt. \end{aligned} \quad (51)$$

To find $\psi_{3/2}(x)$, we use the integral representation for $\Phi(z, \frac{3}{2})$,

$$\Phi\left(z, \frac{3}{2}\right) = \Gamma\left(\frac{3}{2}\right)^{-1} \int_0^{\infty} \frac{\sqrt{t}}{e^t - z} dt \quad (52)$$

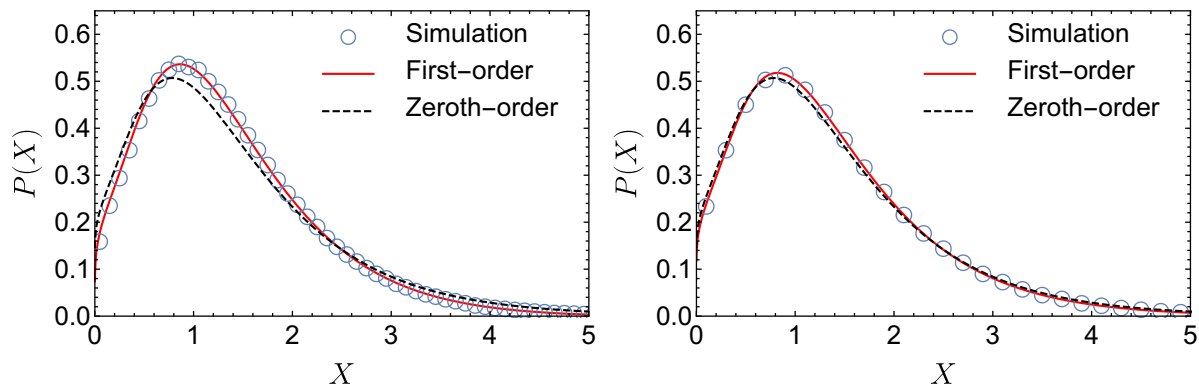


Figure 3. Probability density of the scaled number of fitness maxima X for $L = 20$ (left panel) and $L = 50$ (right panel). Simulation results are compared to the asymptotic density $P(x)$ (38) and the first-order $O(1/L)$ correction (54).

and perform the contour integral along the contour in figure 1, which gives

$$\psi_{3/2}(x) = \frac{2}{\sqrt{\pi}} \int_1^\infty \frac{\exp(-wx) \sqrt{\ln w}}{w} dw = \frac{2}{\sqrt{\pi}} \int_0^\infty \sqrt{t} \exp(-xe^t) dt. \quad (53)$$

Hence the correction to the probability density $P(x)$ is given by

$$\Delta P(x) = -\frac{3S}{4L} \sum_{l=0}^{\infty} \frac{\Psi(x2^l)}{(2; 2)_l}, \quad (54)$$

where

$$\Psi(x) = \frac{1}{\sqrt{\pi}} \int_0^\infty dt \frac{\exp(-xe^t)}{\sqrt{t}} (2t - 1 - 2xe^t + x^2 e^{2t}). \quad (55)$$

In figure 3, we compare our prediction with simulations, which shows an excellent agreement already for $L = 20$. The simulation method is explained in Appendix H.

5.3. One-dimensional AFHM and the number partitioning problem

In Appendix I the calculation of the probability density is repeated for the one-dimensional AFHM, and the limiting distribution is found to be

$$P_{\text{AFHM}}(x) = S \sum_{l=0}^{\infty} \frac{2^l}{(2; 2)_l} \exp(-2^l x). \quad (56)$$

Again the behaviour for large x is determined by the $l = 0$ term and is simply exponential in this case. However, the behaviour for small x differs markedly from that of FGM. In fact the expression (56) can be shown to have vanishing derivatives of all orders at $x = 0$, which implies an essential singularity at the origin (figure 4). Thus, whereas small values of X are relatively likely for FGM, they are very rare in the AFHM.

The one-dimensional AFHM is closely related to the number partitioning problem (NPP) [30, 31]. In this problem one asks for the optimal subdivision of L positive

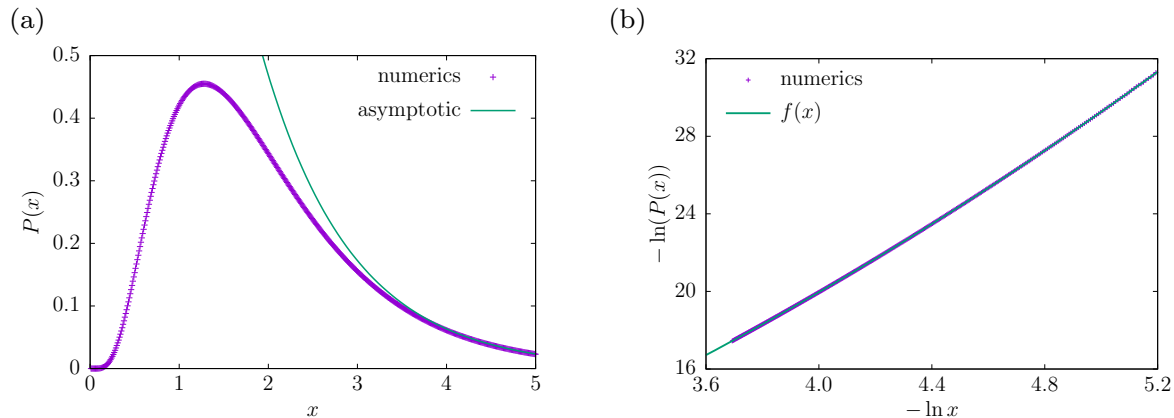


Figure 4. (a) Probability density $P(x)$ of the scaled number of fitness maxima for the AFHM with $n = 1$ (symbols) together with the exponential behaviour Se^{-x} for large x (line), where S is defined in (37). The function $P(x)$ is obtained by numerical summation of (56). (b) Plot of $-\ln(P(x))$ vs. $-\ln x$ (symbols). The fitting function $f(x) = ax^2 + bx + c$ with $a = 0.851$, $b = 1.64$, $c = -0.215$ (line) is almost indistinguishable from the numerical data (see Appendix I for details).

random numbers ξ_i , $i = 1, \dots, L$ into two subsets $\mathcal{S}_1, \mathcal{S}_2$ such that the difference Δ between the sums of the ξ_i over the subsets is as small as possible. Setting $s_i = 1$ if $i \in \mathcal{S}_1$ and $s_i = -1$ if $i \in \mathcal{S}_2$ the difference can be written as

$$\Delta = \sum_{i \in \mathcal{S}_1} \xi_i - \sum_{j \in \mathcal{S}_2} \xi_j = \sum_{i=1}^L \xi_i s_i, \quad (57)$$

and $|\Delta|^2$ is seen to be proportional to the one-dimensional AFHM Hamiltonian. In [30] the expected number of local minima of $|\Delta|^2$ was computed for the case when the ξ_i are uniform random variable on the interval $[0, 1]$. The result

$$\langle \mathcal{N} \rangle_{\text{NPP}} \sim \sqrt{\frac{24}{\pi}} \frac{2^L}{L^{3/2}}, \quad L \rightarrow \infty, \quad (58)$$

displays the same scaling with L that we have obtained for FGM and AFHM. The prefactor can be obtained from our result (I.11) for the AFHM using the rescaling (C.8) with $\omega^2 = \frac{1}{12}$ and $p(0) = 1$ for the uniform distribution.

6. Correlation between local maxima

In this section we consider the conditional probability $P(\sigma_2|\sigma_1)$ that a genotype σ_2 is a local maximum, given that σ_1 is also a local maximum, for FGM with a one-dimensional phenotype space. This is to be compared to the unconditional probability $P_1(\sigma_2)$ that σ_2 is a local maximum. Using the notation in section 4, we define

$$C(\sigma_1, \sigma_2) = \frac{P(\sigma_2|\sigma_1)}{P_1(\sigma_2)} = \frac{P_2(\sigma_1, \sigma_2)}{P_1(\sigma_1)P_1(\sigma_2)}. \quad (59)$$

Due to permutation symmetry, P_2 depends only on the following four parameters:

$$\begin{aligned} u_0 &\equiv \sum_{i=1}^L [1 - \tau_i(\sigma_1)] [1 - \tau_i(\sigma_2)], & u_1 &\equiv \sum_{i=1}^L [1 - \tau_i(\sigma_1)] \tau_i(\sigma_2), \\ u_2 &\equiv \sum_{i=1}^L \tau_i(\sigma_1) [1 - \tau_i(\sigma_2)], & u_3 &\equiv \sum_{i=1}^L \tau_i(\sigma_1) \tau_i(\sigma_2). \end{aligned} \quad (60)$$

Obviously, $u_0 + u_1 + u_2 + u_3 = L$. These parameters can be interpreted as follows: u_0 is the number of shared non-mutated sites (i.e., the number of 00 pairs in a sequence alignment), u_3 is the number of shared mutated sites (11 pairs), u_1 is the number of sites that do not have mutations in σ_1 but have mutations in σ_2 (01 pairs), and u_2 is the number of sites that do not have mutations in σ_2 but have mutations in σ_1 (10 pairs); see (J.1) for a pictorial representation. As shown in Appendix J, for large u_i the probabilities P_1 and P_2 can be approximated as

$$P_1(\sigma_1) = \frac{1}{L\sqrt{d_1}}, \quad P_1(\sigma_2) = \frac{1}{L\sqrt{d_2}}, \quad (61)$$

$$P_2(\sigma_1, \sigma_2) = \frac{3}{(L + d_{12})(2L - d_{12})(d_1 d_2 - u_3^2)^{1/2}}, \quad (62)$$

which yields

$$C(\sigma_1, \sigma_2) = 3 \left(1 + \frac{d_{12}}{L}\right)^{-1} \left(2 - \frac{d_{12}}{L}\right)^{-1} \left(1 - \frac{u_3^2}{d_1 d_2}\right)^{-1/2} \quad (63)$$

with $d_1 = u_2 + u_3$, $d_2 = u_1 + u_3$, and $d_{12} = u_1 + u_2$. Here d_i is the Hamming distance from the wild type to σ_i and d_{12} is the Hamming distance between σ_1 and σ_2 .

To discuss the significance of (61), (62), and (63), we first consider two genotypes with $d_1/L \approx d_2/L \approx d_{12}/L \approx \frac{1}{2}$ for large L , or $u_i/L \approx \frac{1}{4}$ for $i = 0, 1, 2, 3$. For this set of values, we get

$$P_1^* = \sqrt{2}L^{-3/2} = \mu_1 L^{-3/2} = \frac{\langle \mathcal{N} \rangle}{2L}, \quad P_2^* = \frac{16}{\sqrt{27}L^3} = \mu_2 L^{-3} = \frac{\langle \mathcal{N}^2 \rangle}{2^{2L}}. \quad (64)$$

This shows that a local maximum is typically located around $d = L/2$ and similarly a typical pair of local maxima is separated by Hamming distance $d_{12} = L/2$, as would be expected for entropic reasons. For two randomly chosen genotypes we therefore have

$$C^* \equiv \frac{P_2^*}{(P_1^*)^2} = \frac{\mu_2}{\mu_1^2} = \frac{8}{\sqrt{27}} \simeq 1.54 > 1 \quad (65)$$

simply because the distribution of the scaled number of maxima has a nonzero width.

Next we observe that when $u_3 = 0$ (no shared mutations), C takes on its minimal value $\frac{4}{3}$ when $d_{12} = \frac{1}{2}L$. As C is an increasing function of u_3 for fixed d_{12} , this constitutes a global lower bound on C ,

$$C(\sigma_1, \sigma_2) \geq C_{\min} = \frac{4}{3} < C^*. \quad (66)$$

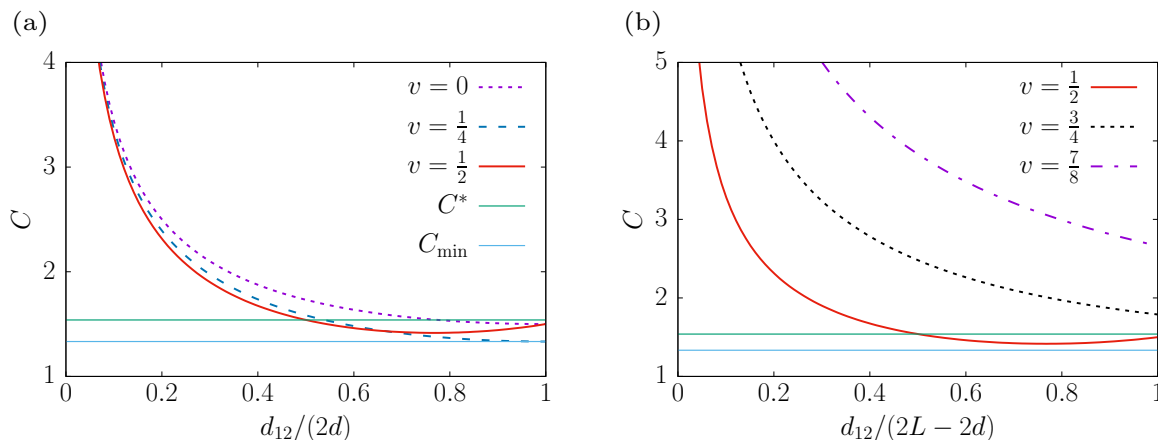


Figure 5. Correlation between two local maxima located at the same distance $d_1 = d_2 = d$ from the wild type. (a) $C(\sigma_1, \sigma_2)$ as a function of $d_{12}/(2d)$ for different values of $v = d/L \leq 1/2$; see (67). Since we are considering the infinite L limit, $v = 0$ does not necessarily mean $d = 0$, but rather that d is small compared to L (for example, $d = \sqrt{L}$). (b) $C(\sigma_1, \sigma_2)$ as a function of $d_{12}/(2L - 2d)$ for different values of $v = d/L \geq 1/2$; see (68). In both panels the random expectation C^* and the lower bound C_{\min} are depicted as horizontal lines.

Two randomly chosen genotypes conditioned to have no shared mutations are thus less likely to be maxima than expected for unconstrained sequences.

It is also instructive to analyse the symmetric case $d_1 = d_2 = d$, where both genotypes are at the same distance from the wild type. Since $d_{12} \leq 2 \min(d, L - d)$, we choose $w \equiv d_{12}/[2 \min(d, L - d)]$ as our free parameter. In terms of w , C can be written as

$$C = \frac{3}{2\sqrt{w}(1 + 2vw)(1 - vw)(2 - w)^{1/2}}, \quad \text{for } v \leq \frac{1}{2}, \quad (67)$$

$$C = \frac{3v}{2\sqrt{w(1 - v)}[1 + 2(1 - v)w][1 - (1 - v)w][(2 + w)v - w]^{1/2}}, \quad \text{for } v \geq \frac{1}{2}, \quad (68)$$

where $v \equiv d/L$. The divergence for $w \ll 1$ shows that nearby maxima are clustered in sequence space, an effect that has been found also in other fitness landscape models [41]. Nevertheless there are regions where maxima effectively repel, in the sense that C is smaller than the random expectation C^* , and moreover the correlations do not always vary monotonically with d_{12} (figure 5).

7. Summary and discussion

In this paper, we studied the distribution of the number \mathcal{N} of local maxima in the genotypic fitness landscapes generated according to Fisher's geometric model (FGM) with phenotypic dimension n . We first examined the connection between FGM and the anti-ferromagnetic Hopfield model (AFHM) with n real-valued patterns, where local fitness maxima correspond to zero-temperature metastable states that are stable under single spin flips. When the phenotypic dimension n and the genotype sequence length

L (corresponding to the number of spins in the AFMH) are jointly taken to infinity at fixed but small ratio $\alpha = n/L$, we find that the exponential growth rate Σ^* of the mean number of maxima is identical for the two models up to $O(\alpha \ln |\ln \alpha|)$.

More detailed results are obtained when the limit $L \rightarrow \infty$ is performed at finite n . In this case, we show that $X = \mathcal{N}L^{1+n/2}/2^L$ is an appropriate rescaled random variable with a well-defined probability density both for FGM and the AFHM. In particular, we derive the exact probability densities $P(X)$ for both models in the case $n = 1$. Despite the identical scaling, the two densities display remarkably different behaviours for small X . Furthermore, we compute the leading finite size correction to the distribution and show that the obtained analytic expression agrees well with simulation results. Finally, we provide a detailed analysis of the pairwise correlations between the positions of local fitness maxima in the one-dimensional FGM, finding a pronounced clustering of maxima at small Hamming distance. To the best of our knowledge these are the first analytic results for the correlation between maxima in a fitness landscape model with nontrivial structure.

The full distribution of fitness maxima has been found only in a few fitness landscape models so far, but already this small number of examples suggests a diverse range of possible scenarios. The simplest genotypic fitness landscape is the House-of-Cards (HoC) model, where fitness values are drawn from a continuous probability distribution and assigned independently to genotypes [42, 43]; the corresponding spin system is known as the Random Energy model [44]. In the HoC model the distribution converges to a Gaussian for large L , with a variance that is proportional to the mean [45, 46]. This implies that the number of maxima \mathcal{N} itself becomes a deterministic (self-averaging) quantity.

Another solvable case is the NK block model, where the L sites of the sequence are subdivided into disjoint subsets of size k . The fitness landscape of each subset is an uncorrelated HoC landscape, and the fitness of the genotype is the sum of the contributions of the subsets [10, 47]. The total number of fitness maxima is then the product of the numbers of maxima of the sublandscapes, and therefore the distribution of \mathcal{N} becomes log-normal in the limit $L \rightarrow \infty$ at fixed k [48]. As a consequence $\ln \mathcal{N}$ is self-averaging, but a scaling form for \mathcal{N} similar to that found here for FGM does not exist, because the moment $\langle \mathcal{N}^m \rangle$ does not scale as the m th power of $\langle \mathcal{N} \rangle$. It would be of interest to investigate the limiting distribution of the number of maxima that arises in this model (as well as in other versions of the NK model [10]) when the joint limit $k, L \rightarrow \infty$ is performed at fixed ratio k/L .

Yet stronger fluctuations in \mathcal{N} are found in FGM when the distance of the wild-type phenotype to the fitness optimum is nonzero and scales as $|\vec{Q}| = qL$. In [19] the exponential growth rate Σ^* of the mean number of maxima was computed as a function of q , and was found to vanish at $q_c \approx 0.924809$. On the other hand, the typical value of $\ln \mathcal{N}$ can be obtained from a thermodynamic calculation of the entropy of the model [49], which shows that the extensive part of $\langle \ln \mathcal{N} \rangle$ vanishes already at $q = \frac{1}{\sqrt{2\pi}} \approx 0.399$. Thus for $0 < q < q_c$, $\ln \langle \mathcal{N} \rangle \gg \langle \ln \mathcal{N} \rangle$ and the self-averaging property breaks down also on

the level of $\ln \mathcal{N}$. Preliminary work on the thermodynamics of the model for general α suggests that this glassy behavior is typical throughout the $\alpha - q$ -phase diagram, such that $\ln \mathcal{N}$ is self-averaging only at the point $\alpha = q = 0$.

From a biological perspective it is of interest to go beyond the assumption of binary genotype sequences and consider models where the number of possible states per site (the number of *alleles*) is $A > 2$ [50, 51]. This modification has opposing effects on the number of fitness maxima. On the one hand, the total number of genotypes increases trivially to A^L , but at the same time the number of conditions that have to be satisfied for a genotype to be a fitness peak also increases. For the HoC model [43] and the NK block model [48] these effects are easily accounted for. However, for FGM the analysis of the multiallelic generalization proposed in [19] is highly nontrivial and will be presented elsewhere [52].

To conclude, FGM is a paradigm for understanding how complex genotypic fitness landscapes arise from combining a simple (linear) genotype-phenotype map with an equally simple (nonlinear but single-peaked) phenotype-fitness map [11, 12]. This paradigm is becoming increasingly relevant for the analysis of large-scale empirical data sets encompassing hundreds of thousands of genetic sequences [53]. Sample-to-sample fluctuations in summary statistics such as the number of fitness peaks constitute a significant obstacle to inference methods aimed at extracting low-dimensional phenotypes from genotype-fitness data [38]. We hope that the present case study can help to address this problem and contribute to the further development of fitness landscape methods in evolutionary genetics.

Acknowledgments

SCP acknowledges support by the Basic Science Research Program through the National Research Foundation of Korea (NRF) funded by the Ministry of Science and ICT (Grant No. 2017R1D1A1B03034878); and by the Catholic University of Korea, research fund 2019. SH and JK acknowledge support by DFG within CRC 680 and CRC 1310. The authors furthermore thank the Regional Computing Center of the University of Cologne (RRZK) for providing computing time on the DFG-funded High Performance Computing (HPC) system CHEOPS.

Appendix A. Small α limit for $\vec{Q} = 0$

As discussed in section 3, FGM with $\vec{Q} = 0$ can be mapped into a certain variant of the AFHM. Here, we perform a direct comparison between the two models in terms of the exponential growth rate of the mean number of maxima Σ^* defined in (13). In our recent study of FGM [19], we have shown that Σ^* is obtained by maximizing the

function $\Sigma(a, b, c)$ with respect to a , b , and c ||, where

$$\Sigma(a, b, c) = -\frac{\alpha}{2} \ln \left(\frac{\alpha^2}{ac + b^2} \right) + \alpha + b - 2c + \ln M, \quad (\text{A.1})$$

$$M \equiv \frac{1}{2} \left[\operatorname{erf} \left(\frac{\alpha + 2b}{\sqrt{2a}} \right) + 1 \right] + \frac{e^{2c}}{2} \left[\operatorname{erf} \left(\frac{\alpha}{\sqrt{2a}} \right) + 1 \right], \quad (\text{A.2})$$

and $\operatorname{erf}(x)$ is the error function. By taking derivatives with respect to each variable, we get

$$\frac{\alpha c}{2(ac + b^2)} - \frac{(\alpha + 2b)X + \alpha Y}{2Ma\sqrt{2\pi a}} = 0, \quad (\text{A.3})$$

$$1 + \frac{\alpha b}{ac + b^2} + \left(\frac{2}{a\pi} \right)^{1/2} \frac{X}{M} = 0, \quad (\text{A.4})$$

$$\frac{a\alpha}{2(ac + b^2)} - \frac{1}{M} \left[\operatorname{erf} \left(\frac{\alpha + 2b}{\sqrt{2a}} \right) + 1 \right] = 0, \quad (\text{A.5})$$

where

$$X \equiv \exp \left(-\frac{(\alpha + 2b)^2}{2a} \right), \quad Y \equiv \exp \left(2c - \frac{\alpha^2}{2a} \right). \quad (\text{A.6})$$

The solution $(a, b, c) = (a^*, b^*, c^*)$ of (A.3), (A.4), and (A.5) determines $\Sigma^* = \Sigma(a^*, b^*, c^*)$.

To find an approximate solution, we first observe that $\Sigma^* = \ln 2$ for $\alpha = 0$ according to (27). Thus for $\alpha \rightarrow 0$, M should approach 2 and the arguments of both error functions in (A.2) should diverge, which suggests (we drop the asterisks for brevity)

$$a = \frac{1}{2}\alpha^2 A(\alpha), \quad (\text{A.7})$$

with $A(\alpha) \rightarrow 0$ as $\alpha \rightarrow 0$.

From (A.5) together with the above observation, we get

$$\frac{a\alpha}{ac + b^2} = 2 + o(1) \rightarrow c + \frac{b^2}{a} = \frac{1}{2}\alpha + o(\alpha), \quad (\text{A.8})$$

from which we conclude that $|b| \ll \alpha$ (accordingly, $\alpha + 2b \approx \alpha$) and $c \ll 1$. Note that because of (A.3) c is positive. Therefore, we have

$$X \approx Y \approx \exp \left(-\frac{1}{A} \right). \quad (\text{A.9})$$

Using (A.8) and (A.9), we can approximate (A.3) and (A.4) as

$$c \approx \frac{\exp(-1/A)}{(4\pi A)^{1/2}}, \quad 1 + \frac{2b}{a} + \frac{2c}{\alpha} \approx 0. \quad (\text{A.10})$$

Since c is at most $O(\alpha)$, b must be $O(a)$, which, along with (A.8) and (A.7), gives

$$c \approx \frac{1}{2}\alpha. \quad (\text{A.11})$$

|| The original equation (46) in [19] used an alternative variational parameter g which is defined as $16g^2c = \alpha^2 - g^2$. However, in our setting $g = 0$, and it is natural to use c since g is simply α .

Thus, (A.10) yields $b \approx -a$ and

$$\frac{\exp(-1/A)}{(\pi A)^{1/2}} \approx \alpha. \quad (\text{A.12})$$

Using successive approximations to solve (A.12), we get

$$\frac{1}{A} = \ln \frac{1}{\alpha\sqrt{\pi}} + \frac{1}{2} \ln \frac{1}{A} \approx \ln \frac{1}{\alpha\sqrt{\pi}} + \frac{1}{2} \ln \left(\ln \frac{1}{\alpha\sqrt{\pi}} \right). \quad (\text{A.13})$$

To find the asymptotic behaviour of Σ^* for small α , we exploit the asymptotics of the error function $\text{erf}(x) \sim 1 - \exp(-x^2)/(\sqrt{\pi}x)$ to write

$$\text{erf} \left(\frac{\alpha + 2b}{\sqrt{2a}} \right) \simeq \text{erf} \left(\frac{\alpha}{\sqrt{2a}} \right) = \text{erf} \left(\frac{1}{\sqrt{A}} \right) \sim 1 - A \frac{\exp(-1/A)}{(\pi A)^{1/2}} \approx 1 - \alpha A, \quad (\text{A.14})$$

where we use (A.12). We can now approximate M as

$$M \approx (2 - \alpha A) \frac{1 + e^{2c}}{2} \approx (2 - \alpha A) \left(1 + \frac{\alpha}{2} \right) \approx 2 + \alpha - \alpha A. \quad (\text{A.15})$$

Using (A.8), (A.12), (A.13), and (A.15), we finally arrive at

$$\begin{aligned} \Sigma^* &\approx \ln 2 + \ln \left(1 + \frac{\alpha(1-A)}{2} \right) - \frac{\alpha}{2} \ln \left(\frac{4}{\alpha A} \right) \approx \ln 2 - \frac{\alpha}{2} \left[\ln \left(\frac{4}{e\alpha A} \right) + A \right] \\ &\approx \ln 2 - \frac{\alpha}{2} \left[\ln \left(-\frac{4 \ln \alpha}{e\alpha} \right) + \frac{1}{2} \ln \left(\frac{e^2}{\pi} \ln \frac{1}{\alpha} \right) \left(\ln \frac{1}{\alpha} \right)^{-1} \right], \end{aligned} \quad (\text{A.16})$$

which is identical, up to $O(\alpha \ln |\ln \alpha|)$, to Σ^* of the AFHM given in equation (37) of [25].

Appendix B. Derivation of (27)

To find the moments of the number of fitness maxima \mathcal{N} , we first have to calculate the expression defined in (25) as

$$S_m \equiv \sum_{\vec{a}} \int_{\mathcal{A}(a)} d\vec{\xi} p(\vec{\xi}) \exp \left(-i\vec{\xi} \cdot \sum_{\beta=1}^m \vec{k}_\beta a_\beta \right), \quad (\text{B.1})$$

where we introduce the short-hand notation

$$\sum_{\vec{a}} = \sum_{a_1=0}^1 \cdots \sum_{a_m=0}^1. \quad (\text{B.2})$$

The integral over the domain $\mathcal{A}(a)$ is expressed as the difference between the same integral over the whole space \mathbb{R}^n and over the complement $\mathbb{R}^n \setminus \mathcal{A}(a)$. Accordingly, S_m is decomposed into two parts as

$$S_m = 2^m F - 2^m K. \quad (\text{B.3})$$

The first term simply corresponds to the characteristic function of $p(\vec{\xi})$, i.e.,

$$F = \frac{1}{2^m} \sum_{\vec{a}} G \left(\sum_{\beta=1}^m \vec{k}_{\beta} a_{\beta} \right), \quad (\text{B.4})$$

where $G(\vec{k}) \equiv \int d\vec{\xi} p(\vec{\xi}) \exp(-i\vec{k} \cdot \vec{\xi})$. The second term is

$$K = \frac{1}{2^m} \sum_{\vec{a}} \int_c d\vec{\xi} p(\vec{\xi}) \exp \left(-i\vec{\xi} \cdot \sum_{\beta=1}^m \vec{k}_{\beta} a_{\beta} \right), \quad (\text{B.5})$$

where \int_c represents the integral over the complement $\mathbb{R}^n \setminus \mathcal{A}(a)$. We can thus rewrite (24) as

$$\langle \mathcal{N}^m \rangle = \frac{2^{mL}}{(2\pi)^{mn}} \int \prod_{\alpha=1}^m d\vec{z}_{\alpha} d\vec{k}_{\alpha} \exp \left[i\vec{k}_{\alpha} \cdot \vec{z}_{\alpha} - iL^{\gamma} \vec{k}_{\alpha} \cdot \vec{q} + L \ln(F - K) \right], \quad (\text{B.6})$$

where we have introduced the scaling relation $\vec{Q} = \vec{q}L^{\gamma}$ with $|\vec{q}| = O(1)$.

The integral (B.6) can now be solved by means of the saddle point method in the limit $L \rightarrow \infty$. Depending on the choice of the scaling of \vec{Q} , the integral forms a saddle point at the scale $|\vec{z}_{\alpha}| \sim O(L)$ or $|\vec{z}_{\alpha}| \sim O(1)$, which determines the typical phenotypes giving rise to local maxima [19]. If the choice $\gamma < 1$ is made, it was shown in [19] that typical realizations of the $\vec{\xi}_i$ can find a subset of phenotypes that are close to the origin, and thus the integral is dominated by the region $|\vec{z}_{\alpha}| \sim O(1)$ and accordingly $|\vec{k}_{\alpha}| = O(L^{-3/2})$. Around this point, F is expanded into

$$\begin{aligned} F &\approx \frac{1}{2^m} \sum_{\vec{a}} \left[1 - \frac{1}{2} \left(\sum_{\beta=1}^m \vec{k}_{\beta} a_{\beta} \right)^2 \right] = \frac{1}{2^m} \left(2^m - \frac{1}{2} \sum_{\alpha,\beta} \vec{k}_{\alpha} \cdot \vec{k}_{\beta} \sum_{\vec{a}} a_{\alpha} a_{\beta} \right) \\ &= 1 - \frac{1}{2^{m+1}} \sum_{\alpha,\beta} \vec{k}_{\alpha} \cdot \vec{k}_{\beta} [\delta_{\alpha\beta} 2^{m-1} + (1 - \delta_{\alpha\beta}) 2^{m-2}] = 1 - \sum_{\alpha,\beta} \vec{k}_{\alpha} \cdot \vec{k}_{\beta} A_{\alpha\beta}, \end{aligned} \quad (\text{B.7})$$

where $A_{\alpha\beta} = \frac{1}{8}(1 + \delta_{\alpha\beta})$. Note that the above approximation is valid as long as the standard deviation of $p(\vec{\xi})$ is finite. In general, the sum over α, β in the last expression is multiplied by the variance of the distribution, which here has been set to unity.

Next, K can be expanded in a similar manner. In the region $|\vec{z}_{\alpha}| \sim O(1)$,

$$K \approx 2^{-m} p(0) V, \quad V = V[\{\vec{z}_{\alpha}\}_{\alpha=1,\dots,m}] \equiv \sum_{\vec{a}} \int_c d\vec{\xi} \sim O(|\vec{z}_{\alpha}|^n). \quad (\text{B.8})$$

Note that the term $i\vec{k}_{\alpha} \cdot \vec{z}_{\alpha}$ is negligible for this choice of γ , which allows the integrals over the \vec{k}_{α} 's and the \vec{z}_{α} 's in (B.6) to be treated independently. The integration over \vec{k} 's are evaluated as follows:

$$\begin{aligned} &\int \prod_{\alpha=1}^m d\vec{k}_{\alpha} \exp \left(-L \sum_{\alpha,\beta} \vec{k}_{\alpha} \cdot \vec{k}_{\beta} A_{\alpha\beta} + iL^{\gamma} \sum_{\alpha} \vec{k}_{\alpha} \cdot \vec{q} \right) \\ &= \left(\frac{8\pi}{L} \right)^{nm/2} \frac{1}{(m+1)^{n/2}} \exp \left(-L^{2\gamma-1} \frac{2m}{m+1} |\vec{q}|^2 \right), \end{aligned} \quad (\text{B.9})$$

where we have used the fact that

$$A_{\mu\nu}^{-1} = 8 \left(\delta_{\mu\nu} - \frac{1}{m+1} \right), \quad \frac{1}{4} \sum_{\mu,\nu} \vec{q}_\mu \cdot \vec{q}_\nu A_{\mu\nu}^{-1} = -\frac{2m}{m+1} |\vec{q}|^2. \quad (\text{B.10})$$

Introducing a symbol μ_m for the remaining integral over \vec{z}_α , we thus obtain (27) with

$$\begin{aligned} \mu_m &= L^m \left(\frac{2^m}{\pi^m(m+1)} \right)^{n/2} \int \prod_{\alpha} d\vec{z}_\alpha \exp[-Lp(0)2^{-m}V] \\ &= \left(\frac{2^m}{\pi^m(m+1)} \right)^{n/2} \int \prod_{\alpha} d\vec{z}_\alpha \exp[-p(0)2^{-m}V], \end{aligned} \quad (\text{B.11})$$

where, in the last equality, we have changed the variables $L^{1/n}z_\alpha^k \mapsto z_\alpha^k$ for all components of \vec{z}_α .

Appendix C. Moments for $n = 1$ and $Q = 0$

In this appendix, we present the exact leading asymptotic behaviour of all moments for the case of $n = 1$ at $Q = 0$. In the following z_α should be understood as a real number which can take negative values rather than the magnitude of the vector $|\vec{z}_\alpha|$. Setting $n = 1$ in (B.11), we write

$$\mu_m = \frac{1}{\sqrt{m+1}} \left(\frac{2}{\pi} \right)^{m/2} \int \prod_{\alpha} dz_\alpha \exp[-p(0)2^{-m}V], \quad (\text{C.1})$$

where

$$\begin{aligned} V &= \sum_{\bar{a}} \int_c dx = 2 \sum_{\bar{a}} [\max(0, -s_1 z_1, \dots, -s_m z_m) - \min(0, -s_1 z_1, \dots, -s_m z_m)] \\ &= 4 \sum_{\bar{a}} \max(0, s_1 z_1, \dots, s_m z_m), \end{aligned} \quad (\text{C.2})$$

with $s_\alpha \equiv 2a_\alpha - 1$. In the above equation, we have used the identities $-\min(0, -s_\alpha z_\alpha) = \max(0, s_\alpha z_\alpha)$ and $\sum_{\bar{a}} \max(0, -s_\alpha z_\alpha) = \sum_{\bar{a}} \max(0, s_\alpha z_\alpha)$.

Since V is invariant under the transformation $z_\alpha \mapsto -z_\alpha$ for each α as well as under all permutations of the indices α , we can write (C.1), after making the change of variables $y_\alpha = p(0)2^{2-m}z_\alpha$, as

$$\begin{aligned} \mu_m &= \frac{2^{m^2}}{\sqrt{m+1}} \left(\frac{2}{\pi} \right)^{m/2} \frac{1}{[4p(0)]^m} 2^m m! \times \\ &\quad \int_0^\infty dy_1 \int_{y_1}^\infty dy_2 \dots \int_{y_{m-1}}^\infty dy_m \exp \left[- \sum_{\bar{a}} \max(0, s_1 y_1, \dots, s_m y_m) \right]. \end{aligned} \quad (\text{C.3})$$

Now the domains of integration with respect to y_α are arranged in such a way that $y_1 < y_2 < \dots < y_m$. Within this ordering, we can establish the following identity

$$\sum_{\bar{a}} \max(0, s_1 y_1, \dots, s_m y_m) = 2^{m-1} y_m + 2^{m-2} y_{m-1} + \dots + 2y_2 + y_1 = \sum_{k=1}^m 2^{k-1} y_k. \quad (\text{C.4})$$

Then, the integrals in (C.3) are computed recursively as follows:

$$I_m(y_{m-1}) = \int_{y_{m-1}}^{\infty} \exp(-2^{m-1}y_m) dy_m = \frac{1}{2^{m-1}} \exp(-2^{m-1}y_{m-1}), \quad (\text{C.5})$$

$$\begin{aligned} I_{m-1}(y_{m-2}) &= \int_{y_{m-2}}^{\infty} \exp(-2^{m-1}y_{m-1}) I_m(y_{m-1}) dy_{m-1} \\ &= \frac{1}{2^{m-1}} \frac{1}{2^{m-1} + 2^{m-2}} \exp[-(2^{m-1} + 2^{m-2})y_{m-2}], \end{aligned} \quad (\text{C.6})$$

and so on. Inserting the value $p(0) = \frac{1}{\sqrt{2\pi}}$ for the Gaussian distribution (2), we thus get

$$\mu_m = \frac{2^{m^2} m!}{\sqrt{m+1}} \prod_{k=1}^m \frac{1}{\sum_{j=1}^k 2^{m-j}} = \frac{2^{m^2} m!}{\sqrt{m+1}} \prod_{k=1}^m \frac{1}{2^m - 2^{m-k}} = \frac{m!}{\sqrt{m+1}} \prod_{k=1}^m \frac{1}{1 - 2^{-k}}. \quad (\text{C.7})$$

The first few moments are $\mu_1 = \sqrt{2}$, $\mu_2 = 16/\sqrt{27}$ and $\mu_3 = 64/7$. For general distributions $p(\xi)$ with zero mean and variance ω^2 the expression (C.7) is multiplied by a factor according to

$$\mu_m \mapsto (2\pi\omega^2 p(0)^2)^{-\frac{m}{2}} \mu_m. \quad (\text{C.8})$$

Appendix D. The q -Pochhammer symbol

This appendix summarises some properties of the q -Pochhammer symbol that are used in this paper. The q -Pochhammer symbol was defined in (31). From the definition, we obtain

$$(a; q)_k = (-1)^k a^k q^{k(k-1)/2} (a^{-1}; q^{-1})_k. \quad (\text{D.1})$$

If $(a; q)_\infty$ exists, we can write

$$\frac{1}{(a; q)_k} = \frac{1}{(a; q)_\infty} \prod_{l=k}^{\infty} (1 - aq^l) = \frac{(aq^k; q)_\infty}{(a; q)_\infty} \quad (\text{D.2})$$

Using (D.2) and the infinite series representation

$$(qx; q)_\infty = \sum_{l=0}^{\infty} \frac{x^l}{(q^{-1}; q^{-1})_l}, \quad (\text{D.3})$$

we can write for $q = \frac{1}{2}$

$$\frac{1}{(\frac{1}{2}; \frac{1}{2})_k} = S \sum_{l=0}^{\infty} \frac{2^{-kl}}{(2; 2)_l}, \quad (\text{D.4})$$

where $S \equiv [(\frac{1}{2}; \frac{1}{2})_\infty]^{-1} \approx 3.462\,7466$.

Let

$$a_k \equiv S \sum_{l=0}^{\infty} \frac{l^k 2^l}{(2; 2)_l} = S \left(x \frac{d}{dx} \right)^k \left(\frac{x}{2}; \frac{1}{2} \right)_\infty \Big|_{x=2}, \quad (\text{D.5})$$

where we have used (D.3) to obtain the differential form. As the sum converges quickly, the partial sum of the first few terms already produces an accurate estimate of a_k . The error of the l_0 th order approximation is given by

$$e_k \equiv S \left| \sum_{l=l_0+1}^{\infty} \frac{l^k 2^l}{(2; 2)_l} \right| \leq S \sum_{l=l_0+1}^{\infty} \frac{l^k 2^l}{|(2; 2)_l|}. \quad (\text{D.6})$$

Since

$$\left| \frac{1}{(2; 2)_l} \right| = 2^{-l(l+1)/2} \prod_{k=1}^l (1 - 2^{-k})^{-1} \leq S 2^{-l(l+1)/2}, \quad (\text{D.7})$$

we have

$$\begin{aligned} e_k &\leq S^2 \sum_{l=l_0+1}^{\infty} l^k 2^{-l(l-1)/2} = S^2 l_0^k \sum_{k=1}^{\infty} \left(1 + \frac{k}{l_0}\right)^k 2^{-(l_0+k)(l_0+k-1)/2} \\ &\leq S^2 l_0^k 2^{-l_0(l_0-1)/2} \sum_{r=1}^{\infty} \exp \left[-\frac{\ln 2}{2} r^2 - \left(\frac{2l_0-1}{2} \ln 2 - \frac{k}{l_0} \right) r \right], \end{aligned} \quad (\text{D.8})$$

where we use that $1+x \leq e^x$ for $x \geq 0$. If we choose l_0 such that $l_0(2l_0-1) \ln 2 - 2k \geq 0$, we get

$$\begin{aligned} e_k &\leq S^2 l_0^k 2^{-(l_0^2+l_0+1)/2} e^{k/l_0} \sum_{r=1}^{\infty} \exp \left(-\frac{\ln 2}{2} r^2 \right) \\ &\leq S^2 l_0^k 2^{-(l_0^2+l_0+1)/2} e^{k/l_0} \int_0^{\infty} dr \exp \left(-\frac{\ln 2}{2} r^2 \right) = S^2 \sqrt{\frac{\pi}{\ln 4}} l_0^k 2^{-(l_0^2+l_0+1)/2} e^{k/l_0}. \end{aligned} \quad (\text{D.9})$$

For example, if we choose $l_0 = 12$ for $k = 5$, we obtain $e_5 \leq 1.6 \times 10^{-17}$.

In particular, we can get exact formulae for $k = 0$ and $k = 1$. Since

$$\sum_{l=0}^{\infty} \frac{2^l}{(2; 2)_l} = \left(1; \frac{1}{2}\right)_{\infty} = 0, \quad (\text{D.10})$$

we trivially have $a_0 = 0$. To find a_1 , we write

$$\left(\frac{x}{2}; \frac{1}{2} \right)_{\infty} \equiv \left(1 - \frac{x}{2}\right) g(x), \quad (\text{D.11})$$

where

$$g(x) = \prod_{l=1}^{\infty} \left(1 - \frac{x}{2^{l+1}}\right). \quad (\text{D.12})$$

Note that $g(2) = S^{-1}$. From this identity, we find

$$a_1 = \frac{x}{g(2)} \frac{d}{dx} \left[\left(1 - \frac{x}{2}\right) g(x) \right] \Big|_{x=2} = -1. \quad (\text{D.13})$$

Appendix E. Another way of finding $P(x)$

We first observe that

$$\frac{1}{\sqrt{m+1}} = \frac{1}{\sqrt{\pi}} \int_0^\infty \frac{e^{-(m+1)t}}{\sqrt{t}} dt. \quad (\text{E.1})$$

Inserting this into (33) yields

$$\begin{aligned} \mathcal{G}(k) &= \frac{1}{\sqrt{\pi}} \sum_{m=0}^{\infty} \frac{(ik)^m}{(\frac{1}{2}; \frac{1}{2})_m} \int_0^\infty \frac{e^{-(m+1)t}}{\sqrt{t}} dt = \frac{1}{\sqrt{\pi}} \int_0^\infty dt \frac{e^{-t}}{\sqrt{t}} \sum_{m=0}^{\infty} \frac{(ike^{-t})^m}{(\frac{1}{2}; \frac{1}{2})_m} \\ &= \frac{1}{\sqrt{\pi}} \int_0^\infty dt \frac{e^{-t}}{\sqrt{t}} \prod_{l=0}^{\infty} \frac{1}{1 - ike^{-t}2^{-l}}, \end{aligned} \quad (\text{E.2})$$

where we have exchanged the orders of summation and integration to arrive at the second equality and used the relation

$$\sum_{m=0}^{\infty} \frac{x^m}{(q; q)_m} = (x; q)_\infty^{-1} \quad (\text{E.3})$$

to obtain the last equality. Hence

$$\begin{aligned} P(x) &= \frac{1}{2\pi} \int_{-\infty}^{\infty} dk \exp(-ikx) \mathcal{G}(k) \\ &= \frac{1}{\sqrt{\pi}} \int_0^\infty dt \frac{e^{-t}}{\sqrt{t}} \int dk \frac{\exp(-ikx)}{2\pi} \prod_{l=0}^{\infty} \frac{1}{1 - ike^{-t}2^{-l}}, \end{aligned} \quad (\text{E.4})$$

where we again changed the order of integration. Since there are poles at $k = -ie^t 2^l$ ($l = 0, 1, 2, \dots$) in the complex k plane, $P(x) = 0$ for $x < 0$. The integral over k for $x > 0$ can be performed as

$$\begin{aligned} &\frac{1}{2\pi} \int dk \exp(-ikx) \prod_{l=0}^{\infty} \frac{1}{1 - ike^{-t}2^{-l}} = e^t \sum_{m=0}^{\infty} 2^m \exp(-2^m x e^t) \prod_{l \neq m} \frac{1}{1 - 2^{m-l}} \\ &= S e^t \sum_{m=0}^{\infty} 2^m \exp(-2^m x e^t) \prod_{l=1}^m \frac{1}{1 - 2^l} = S e^t \sum_{m=0}^{\infty} 2^m \exp(-2^m x e^t) \frac{1}{(2; 2)_m}, \end{aligned} \quad (\text{E.5})$$

which gives

$$\begin{aligned} P(x) &= \frac{S}{\sqrt{\pi}} \sum_{m=0}^{\infty} \frac{2^m}{(2; 2)_m} \int_0^\infty dt \frac{\exp(-2^m x e^t)}{\sqrt{t}} = \frac{S}{\sqrt{\pi}} \sum_{m=0}^{\infty} \frac{2^m}{(2; 2)_m} \int_1^\infty dt \frac{\exp(-2^m x t)}{t \sqrt{\ln t}} \\ &\equiv S \sum_{m=0}^{\infty} \frac{2^m}{(2; 2)_m} \psi(2^m x), \end{aligned} \quad (\text{E.6})$$

where

$$\psi(x) \equiv \frac{1}{\sqrt{\pi}} \int_1^\infty \frac{e^{-xt}}{t \sqrt{\ln t}} dt = \int_0^\infty \frac{\exp(-x e^t)}{\sqrt{\pi t}} dt \quad (\text{E.7})$$

in agreement with (43). To confirm, we calculate the m th moment μ_m from (E.6) as

$$\begin{aligned}\mu_m &\equiv \int_0^\infty x^m P(x) dx = \frac{S}{\sqrt{\pi}} \sum_{p=0}^\infty \frac{2^p}{(2; 2)_p} \int_0^\infty \frac{dt}{\sqrt{t}} \int_0^\infty x^m \exp(-2^p e^t x) dx \\ &= m! \frac{S}{\sqrt{\pi}} \sum_{p=0}^\infty \frac{2^p}{(2; 2)_p} \int_0^\infty \frac{dt}{\sqrt{t}} 2^{-p(m+1)} e^{-(m+1)t} \\ &= \frac{m!}{\sqrt{m+1}} S \sum_{p=0}^\infty \frac{2^{-mp}}{(2; 2)_p} = \frac{m!}{\sqrt{m+1}} \frac{(2^{-m-1}; \frac{1}{2})_\infty}{(\frac{1}{2}; \frac{1}{2})_\infty} = \frac{m!}{\sqrt{m+1} (\frac{1}{2}; \frac{1}{2})_m},\end{aligned}\quad (\text{E.8})$$

which is the desired result.

Appendix F. Asymptotic behaviour of $P(x)$

When $x \gg 1$, we can approximate (43) as

$$\begin{aligned}\psi(x) &= \frac{1}{\sqrt{\pi}} e^{-x} \int_0^\infty \frac{e^{-xt}}{(1+t)\sqrt{\ln(1+t)}} dt \approx \frac{1}{\sqrt{\pi}} e^{-x} \left[\int_0^\infty \frac{e^{-xt}}{\sqrt{t}} dt + O(e^{-x}) \right] \\ &= \frac{e^{-x}}{\sqrt{x}} + O(e^{-2x})\end{aligned}\quad (\text{F.1})$$

Since the terms with $l \geq 1$ in (38) contribute at most $O(e^{-2x})$, the leading behaviour of $P(x)$ is Se^{-x}/\sqrt{x} .

For small x , we write $\psi(x) = (I_1 + I_2 + I_3)/\sqrt{\pi}$ with

$$\begin{aligned}I_1 &= \int_0^x \frac{\exp(-e^{t-x})}{\sqrt{t}} dt = \int_0^x \frac{\exp(-e^{-t})}{\sqrt{\chi - t}} dt, \\ I_2 &= \int_0^x \frac{\exp(-e^t)}{\sqrt{t + \chi}} dt, \quad I_3 = \int_x^\infty \frac{\exp(-e^t)}{\sqrt{t + \chi}} dt,\end{aligned}\quad (\text{F.2})$$

and $\chi = -\ln x$. I_3 is at most $O(e^{-x})$ because

$$I_3 = \int_0^\infty \frac{\exp(-e^{t+\chi})}{\sqrt{t + 2\chi}} dt \leq \frac{1}{\sqrt{2\chi}} \int_0^\infty \exp(-te^\chi) dt = \frac{e^{-\chi}}{\sqrt{2\chi}}.\quad (\text{F.3})$$

Next, we find the asymptotic behaviour of I_2 as

$$\begin{aligned}I_2 &= \frac{1}{\sqrt{\chi}} \int_0^x \exp(-e^t) \left(1 + \frac{t}{\chi}\right)^{-1/2} dt = \frac{1}{\sqrt{\chi}} \int_0^x \exp(-e^t) \left[1 - \frac{t}{2\chi} + O(\chi^{-2})\right] dt \\ &= \frac{1}{\sqrt{\chi}} \left[\lambda_1 - \frac{\lambda_2}{\chi} + O(\chi^{-2}) \right],\end{aligned}\quad (\text{F.4})$$

where

$$\lambda_1 = \int_0^\infty \exp(-e^t) dt, \quad \lambda_2 = \frac{1}{2} \int_0^\infty t \exp(-e^t) dt,\quad (\text{F.5})$$

and we have used

$$\int_\chi^\infty \frac{t^n}{\exp(e^t)} dt = \int_0^\infty \frac{(\chi + t)^n}{\exp(e^{\chi+t})} dt \leq \chi^n \int_0^\infty \exp\left(-\left(e^\chi - \frac{n}{\chi}\right)t\right) dt = O(e^{-\chi}).\quad (\text{F.6})$$

The leading behaviour of ψ comes from I_1 ,

$$\begin{aligned}
 I_1 &= 2\sqrt{\chi - t} \exp(-e^{-t}) \Big|_{t=0}^x + 2 \int_0^x \sqrt{\chi - t} \exp(-t - e^{-t}) dt \\
 &= \frac{2}{e} \sqrt{\chi} + 2\sqrt{\chi} \int_0^x \exp(-t - e^{-t}) (1 - t/\chi)^{1/2} dt \\
 &\approx \frac{2}{e} \sqrt{\chi} + 2\sqrt{\chi} \int_0^x \exp(-t - e^{-t}) \left(1 - \frac{t}{2\chi} - \frac{t^2}{8\chi^2}\right) dt \\
 &= 2\sqrt{\chi} - 2\sqrt{\chi} \int_0^\infty \exp(-t - e^{-t}) \left(\frac{t}{2\chi} + \frac{t^2}{8\chi^2}\right) dt = 2\sqrt{\chi} - \frac{\lambda_3}{\sqrt{\chi}} - \frac{\lambda_4}{\chi^{3/2}}, \tag{F.7}
 \end{aligned}$$

with

$$\begin{aligned}
 \lambda_3 &= \int_0^\infty t \exp(-t - e^{-t}) dt = \int_{-\infty}^\infty t \exp(-t - e^{-t}) dt - \int_{-\infty}^0 t \exp(-t - e^{-t}) dt, \\
 &= \gamma + \int_0^\infty t \exp(t - e^t) dt = \gamma - t \exp(-e^t) \Big|_0^\infty + \int_0^\infty \exp(-e^t) dt = \gamma + \lambda_1, \tag{F.8}
 \end{aligned}$$

$$\begin{aligned}
 \lambda_4 &= \int_0^\infty \frac{t^2}{4} \exp(-t - e^{-t}) dt = \int_{-\infty}^\infty \frac{t^2}{4} \exp(-t - e^{-t}) dt - \int_{-\infty}^0 \frac{t^2}{4} \exp(-t - e^{-t}) dt \\
 &= \frac{\gamma^2}{4} + \frac{\pi^2}{24} - \int_0^\infty \frac{t^2}{4} \exp(t - e^t) dt \\
 &= \frac{\gamma^2}{4} + \frac{\pi^2}{24} + \frac{t^2}{4} \exp(-e^t) \Big|_{t=0}^\infty - \frac{1}{2} \int_0^\infty t \exp(-e^t) dt = \frac{\gamma^2}{4} + \frac{\pi^2}{24} - \lambda_2, \tag{F.9}
 \end{aligned}$$

where $\gamma \approx 0.5772$ is the Euler-Mascheroni number. Hence the asymptotic behaviour of $\psi(x)$ is

$$\psi(x) = \frac{2}{\sqrt{\pi}} \sqrt{\chi} - \frac{\gamma}{\sqrt{\pi\chi}} - \left(\frac{\gamma^2}{4} + \frac{\pi^2}{24}\right) \frac{1}{\sqrt{\pi\chi^{3/2}}} = \frac{2}{\sqrt{\pi}} \sqrt{\chi} - \frac{\gamma}{\sqrt{\pi\chi}} - \frac{\lambda}{\sqrt{\pi\chi^{3/2}}}, \tag{F.10}$$

where $\lambda \approx 0.494\,528$. Since

$$\begin{aligned}
 \sqrt{\pi}\psi(2^l x) &= 2(\chi - l \ln 2)^{1/2} - \gamma(\chi - l \ln 2)^{-1/2} - \lambda(\chi - l \ln 2)^{-3/2} \\
 &= 2\sqrt{\chi} - \frac{l \ln 2 + \gamma}{\sqrt{\chi}} + \chi^{-3/2} \left(-\lambda - \frac{1}{4} l^2 \ln^2 2 - \frac{1}{2} \gamma l \ln 2\right) \\
 &\quad - \frac{1}{8} \chi^{-5/2} (l^3 \ln^3 2 + 3\gamma l^2 \ln^2 2 + 12\lambda l \ln 2), \tag{F.11}
 \end{aligned}$$

we get

$$\begin{aligned}
 P(x) &\approx \frac{\ln 2}{\sqrt{\pi}} \chi^{-1/2} - \frac{a_2 \ln^2 2 - 2\gamma \ln 2}{4\sqrt{\pi}} \chi^{-3/2} + \frac{12\lambda \ln 2 - 3\gamma a_2 \ln^2 2 - a_3 \ln^3 2}{8\sqrt{\pi}} \chi^{-5/2} \\
 &= \frac{\ln 2}{\sqrt{-\pi \ln x}} \left(1 + \frac{0.094\,944}{\ln x} + \frac{0.150\,994}{\ln^2 x}\right). \tag{F.12}
 \end{aligned}$$

Appendix G. Finite size corrections to $\langle \mathcal{N}^m \rangle$ for $n = 1$

In this appendix, we compute the finite size corrections to (27) for $n = 1$ and $q = 0$. To this end, we expand F defined in (B.4) up to fourth order of k ,

$$F \approx 1 - P + B, \quad P \equiv \sum_{\alpha, \beta} k_\alpha A_{\alpha\beta} k_\beta, \quad B \equiv \frac{1}{2m} \frac{1}{8} \sum_{\bar{a}} \left(\sum_{\alpha} k_\alpha a_\alpha \right)^4. \quad (\text{G.1})$$

The quantity B can be expressed as

$$\begin{aligned} 2^{m+3} B &= \sum_{j_1} k_{j_1}^4 2^{m-1} + \sum_{j_1 \neq j_2} k_{j_1}^3 k_{j_2} 2^{m-2} \binom{4}{3} + \sum_{j_1 < j_2} k_{j_1}^2 k_{j_2}^2 2^{m-2} \binom{4}{2} \\ &+ \sum_{j_1} \sum_{j_2 < j_3, j_1 \neq j_2, j_3} k_{j_1}^2 k_{j_2} k_{j_3} 2^{m-3} \binom{4}{2} 2 + \sum_{j_1 < j_2 < j_3 < j_4} k_{j_1} k_{j_2} k_{j_3} k_{j_4} 2^{m-4} 4!. \end{aligned} \quad (\text{G.2})$$

Expanding the higher orders up to $O(k_i^4)$ and $O(z_i^2)$, we have for large L

$$\begin{aligned} \langle \mathcal{N}^m \rangle &= \frac{2^{mL}}{(2\pi)^m} \int \prod_{i=1}^m dz_i dk_i \exp [L \ln (1 - P + B - K)] \\ &= \frac{2^{mL}}{(2\pi)^m} \int \prod_{i=1}^m dz_i dk_i \exp [-L(P + K)] \left(1 + BL - \frac{LK^2}{2} - LKP - \frac{LP^2}{2} \right). \end{aligned} \quad (\text{G.3})$$

The terms in the parenthesis are simply a collection of multi-variate polynomials of k_i 's. They are evaluated on a case-by-case basis using the following formulae:

$$\begin{aligned} \int \prod_{i=1}^m dk_i e^{-LP} k_j^4 &= \frac{48m^2}{L^2(m+1)^2} \frac{1}{L^{m/2}} \sqrt{\frac{(8\pi)^m}{m+1}}, \\ \int \prod_{i=1}^m dk_i e^{-LP} k_{j_1}^3 k_{j_2} &= -\frac{48m}{L^2(m+1)^2} \frac{1}{L^{m/2}} \sqrt{\frac{(8\pi)^m}{m+1}}, \\ \int \prod_{i=1}^m dk_i e^{-LP} k_{j_1}^2 k_{j_2}^2 &= \frac{16(m^2+2)}{L^2(m+1)^2} \frac{1}{L^{m/2}} \sqrt{\frac{(8\pi)^m}{m+1}}, \\ \int \prod_{i=1}^m dk_i e^{-LP} k_{j_1}^2 k_{j_2} k_{j_3} &= -\frac{16(m-2)}{L^2(m+1)^2} \frac{1}{L^{m/2}} \sqrt{\frac{(8\pi)^m}{m+1}}, \\ \int \prod_{i=1}^m dk_i e^{-LP} k_{j_1} k_{j_2} k_{j_3} k_{j_4} &= \frac{48}{L^2(m+1)^2} \frac{1}{L^{m/2}} \sqrt{\frac{(8\pi)^m}{m+1}}, \end{aligned} \quad (\text{G.4})$$

where the indices of k in the integrals on the left-hand side are assumed to be different. Integrating out the k_i in (G.3), we get

$$\begin{aligned} \langle \mathcal{N}^m \rangle &= \frac{2^{mL}}{(2\pi)^m} \frac{1}{L^{m/2}} \sqrt{\frac{(8\pi)^m}{m+1}} \int \prod_{i=1}^m dz_i \exp(-LK) \\ &\times \left[1 + \frac{3m(m^2+m+2)}{8L(m+1)} - \frac{LK^2}{2} - K \frac{m}{2} - \frac{m(m+2)}{8L} \right]. \end{aligned} \quad (\text{G.5})$$

Finally, using (C.7)

$$\int \prod_{i=1}^m dz_i \exp(-LK) = \frac{m!}{L^m} \left(\frac{\pi}{2}\right)^{m/2} Q_m \quad (\text{G.6})$$

with $Q_m = [(\frac{1}{2}; \frac{1}{2})_m]^{-1}$, we have

$$\langle \mathcal{N}^m \rangle = Q_m \frac{m! 2^{Lm} L^{-3m/2}}{\sqrt{m+1}} \left[1 - \frac{3m^2(m+2)}{4L(m+1)} \right]. \quad (\text{G.7})$$

Appendix H. Numerical estimate of $P(X)$ for large L

The probability density $P(X)$ of the rescaled random variable (28) can be computed by counting the number of local maxima for many different fitness landscape realizations. We will refer to this algorithm as the exact enumeration (EE) method. Since the number of genotypes increases exponentially with L , the EE method becomes unfeasible for sufficiently large L . To circumvent this difficulty, we employ a trick to count the number of local maximum for a given fitness landscape. This appendix explains our numerical method used for $n = 1$, but the extension to higher dimensions is straightforward.

Since the number of local maxima is on average $\sim 2^L L^{-3/2}$, the probability of a randomly chosen genotype being a local maximum is $\sim L^{-3/2}$. For a given fitness landscape, we choose M genotypes randomly and check if the chosen genotype is a local maximum. If there are m local maxima out of M randomly chosen genotypes, we evaluate X as

$$X \approx \frac{m}{M} L^{3/2}, \quad (\text{H.1})$$

because $\mathcal{N}/2^L$ is the probability that a randomly chosen genotype is a local maximum.

We choose M such that the bin size is larger than the expected statistical error of the Monte Carlo method. With 99% probability, m should lie in the interval

$$|m - Mp| < 3\sqrt{Mp}, \quad (\text{H.2})$$

where $p = XL^{-3/2}$. Accordingly,

$$\left| \frac{m}{M} L^{3/2} - X \right| < 3\sqrt{\frac{XL^{3/2}}{M}}. \quad (\text{H.3})$$

Notice that for $M = 10^5 L^{3/2}$ the statistical error is about 0.01 when $X \approx 1$. Thus, in simulations, we set $M = 10^5 L^{3/2}$ and choose the bin size 0.01.

When M is smaller than 2^L , this Monte Carlo approach is more efficient than the EE method. As a rule of thumb, the Monte Carlo method is found to be more efficient than the EE method if $L \geq 24$.

Appendix I. Anti-ferromagnetic Hopfield model for finite n

In this section, we present an analytic expression for the moments of the number \mathcal{N} of local energy minima of the AFHM for finite n and derive the full distribution for $n = 1$. To exploit the similarity to FGM we rewrite the Hamiltonian (7) in the form

$$H_{\text{AFHM}}(\sigma) = \frac{1}{4L} |\vec{z}(\sigma)|^2, \quad \vec{z}(\sigma) \equiv \sum_i \vec{\xi}_i s_i(\sigma), \quad (\text{I.1})$$

where σ now denotes a configuration of Ising spins $s_i \pm 1$ and the $\vec{\xi}_i$'s are i.i.d. random variables with a joint distribution $p(\vec{\xi})$. Since the calculations are largely analogous to those for FGM, we just sketch the procedure and present the results.

The condition for a spin configuration σ_α to be a local maximum is ($i = 1, 2, \dots, L$)

$$\left| \vec{z}_\alpha - 2s_i \vec{\xi}_i \right| = \left| 2\vec{\xi}_i - s_i \vec{z}_\alpha \right| > |\vec{z}_\alpha|, \quad (\text{I.2})$$

where $\vec{z}_\alpha \equiv \vec{z}(\sigma_\alpha)$. Thus the condition for m configurations to be simultaneous local minima can be written as

$$\vec{\xi}_i \in \tilde{\mathcal{A}}_i \equiv \bigcap_{\alpha=1}^m \mathcal{D} \left[\frac{1}{2} s_{i,\alpha} \vec{z}_\alpha \right], \quad (\text{I.3})$$

where \mathcal{D} is defined in (20). By replacing $\tau_i \mapsto s_i$ and $\mathcal{A} \mapsto \tilde{\mathcal{A}}$ in the calculations for FGM, it is straightforward to find the m th moment of \mathcal{N} , which is given by

$$\langle \mathcal{N}^m \rangle = \int_{\mathbb{R}^n} \prod_{\alpha=1}^m \frac{d\vec{z}_\alpha d\vec{k}_\alpha}{(2\pi)^n} \exp\left(i\vec{k}_\alpha \cdot \vec{z}_\alpha\right) (S_m)^L \quad (\text{I.4})$$

with

$$S_m \equiv \sum_{\vec{a}} \int_{\tilde{\mathcal{A}}(\vec{a})} d\vec{\xi} p(\vec{\xi}) \exp\left(-i\vec{\xi} \cdot \sum_{\beta=1}^m \vec{k}_\beta a_\beta\right), \quad \sum_{\vec{a}} = \sum_{a_1=-1}^1 \cdots \sum_{a_m=-1}^1, \quad (\text{I.5})$$

and the domain of integration

$$\tilde{\mathcal{A}}(\vec{a}) \equiv \bigcap_{\alpha=1}^m \mathcal{D} \left[\frac{1}{2} a_\alpha \vec{z}_\alpha \right]. \quad (\text{I.6})$$

Note that a_α now takes the values ± 1 .

The calculation of S_m is almost identical to that in Appendix B. Decomposing S_m into two parts

$$S_m = 2^m \tilde{F} - 2^m \tilde{K},$$

$$\tilde{F} = \frac{1}{2^m} \sum_{\vec{a}} G \left(\sum_{\beta=1}^m \vec{k}_\beta a_\beta \right), \quad \tilde{K} = \frac{1}{2^m} \sum_{\vec{a}} \int_c d\vec{\xi} p(\vec{\xi}) \exp\left(-i\vec{\xi} \cdot \sum_{\beta=1}^m \vec{k}_\beta a_\beta\right), \quad (\text{I.7})$$

where $G(\vec{k})$ is the Fourier transform of $p(\vec{\xi})$ and \int_c represents the integral over the complement $\mathbb{R}^n \setminus \tilde{\mathcal{A}}(a)$, we can write

$$\langle \mathcal{N}^m \rangle = \frac{2^{mL}}{(2\pi)^{mn}} \int \prod_{\alpha=1}^m d\vec{z}_\alpha d\vec{k}_\alpha \exp \left[i\vec{k}_\alpha \cdot \vec{z}_\alpha + L \ln(\tilde{F} - \tilde{K}) \right]. \quad (\text{I.8})$$

Repeating the same procedure as in Appendix B, we get

$$\begin{aligned} \tilde{F} &\approx \frac{1}{2^m} \sum_{\vec{a}} \left[1 - \frac{1}{2} \left(\sum_{\beta=1}^m \vec{k}_\beta a_\beta \right)^2 \right] = \frac{1}{2^m} \left(2^m - \frac{1}{2} \sum_{\alpha,\beta} \vec{k}_\alpha \cdot \vec{k}_\beta \sum_{\vec{a}} a_\alpha a_\beta \right) \\ &= 1 - \frac{1}{2^{m+1}} \sum_{\alpha,\beta} \vec{k}_\alpha \cdot \vec{k}_\beta \delta_{\alpha\beta} 2^m = 1 - \frac{1}{2} \sum_{\alpha} \vec{k}_\alpha^2, \\ \tilde{K} &\approx 2^{-m} p(0) \tilde{V}, \quad \tilde{V} \equiv \sum_{\vec{a}} \int_c d\vec{\xi} \sim O(|\vec{z}_\alpha|^n). \end{aligned} \quad (\text{I.9})$$

Note that $\tilde{V} = V(\vec{z}/2)$ and, accordingly, $\tilde{K} \approx K 2^{-nm}$, where V and K are defined in (B.8). Integration over the \vec{k}_α 's followed by the integration over the \vec{z}_α 's gives

$$\langle \mathcal{N}^m \rangle \approx \left[\frac{2^L}{(2\pi L)^{n/2}} \right]^m \int \prod_{\alpha} d\vec{z}_\alpha e^{-L\tilde{K}} = \left(\frac{2^L}{L^{1+n/2}} \right)^m (m+1)^{n/2} \mu_m, \quad (\text{I.10})$$

where we have changed the variables $L^{1/n} z_\alpha^k / 2 \mapsto z_\alpha^k$ and μ_m is defined in (B.11).

Since the explicit form of μ_m for $n = 1$ is known, the moments for the one-dimensional AFHM are given by

$$\langle \mathcal{N}^m \rangle \approx \left(\frac{2^L}{L^{3/2}} \right)^m Q_m m!, \quad (\text{I.11})$$

where Q_m is defined in (30). Defining again the rescaled random variable X through (32) for $L \rightarrow \infty$, we can write down its generating function as

$$\begin{aligned} \mathcal{G}(k) &= \sum_{m=0}^{\infty} Q_m (ik)^m = S \sum_{m=0}^{\infty} (ik)^m \sum_{l=0}^{\infty} \frac{2^{-lm}}{(2; 2)_l} \\ &= S \sum_{l=0}^{\infty} \frac{1}{(2; 2)_l} \sum_{m=0}^{\infty} (ik 2^{-l})^m = S \sum_{l=0}^{\infty} \frac{1}{(2; 2)_l} \frac{1}{1 - ik 2^{-l}}, \end{aligned} \quad (\text{I.12})$$

where the analytic continuation has been easily attained. It is now straightforward to find the probability density $P(x)$, which is given by (56) in the main text.

Next we discuss the asymptotic behaviour of $P(x)$. For large x the term with $l = 0$ dominates, which gives $P(x) \sim S e^{-x}$. To find the asymptotics for small x , we first note that $P(0) = S(1; \frac{1}{2})_\infty = 0$; see (D.3). In fact, the k th derivative of $P(x)$ at $x = 0$ is $P^{(k)}(0) = (-1)^k S(2^{k-1}; \frac{1}{2})_\infty = 0$, so $P(x)$ near $x = 0$ is hardly discernible from 0. For small $0 < x \ll 1$, the dominant contribution is expected when $2^l x \leq 1$, or $l \leq -\ln x / \ln 2 \equiv l_x$. By approximating $\exp(-2^l x) \approx \theta(l_x - l)$, we have

$$P(x) \approx \left| -S \sum_{l=l_x}^{\infty} \frac{2^l}{(2; 2)_l} \right| \approx S 2^{-l_x(l_x+3)/2} = \exp(-a(\ln x)^2 + b \ln x + c), \quad (\text{I.13})$$

where we use that $\sum_{l=0}^{\infty} \frac{2^l}{(2;2)_l} = 0$, $2^{-lx} = x$, and we neglect the sign because $P(x)$ should be positive. Although we cannot find an analytic form of the parameters a and b , fitting gives a reasonable result with $a = 0.851$, $b = 1.64$, $c = -0.215$. Figure 4 shows the probability density in comparison to the asymptotic behaviour.

As a minimal check of the validity of these results, we calculated a few moments using Monte Carlo simulations along the lines of Appendix H. Note that $\langle (XL^{-3/2})^m \rangle$ is the probability that m randomly chosen configurations are all local minima for a random Hamiltonian. To calculate moments, we first generate L random variables ξ_i , and then choose one set of m random configurations, to check if these configurations are all local minima. If e sets of configurations are found to be local minima among E such attempts (that is, E random Hamiltonians), we estimate $\langle X^m \rangle$ as $L^{3m/2}e/E$. For $L = 500$, we get $\langle X \rangle \approx 1.996$ ($E = 2 \times 10^{10}$) and $\langle X^2 \rangle \approx 5.29$ ($E = 4 \times 10^{11}$), which should be compared to the prediction for infinite L , $\langle X \rangle = 2$ and $\langle X^2 \rangle = \frac{16}{3} \approx 5.33$. Considering that the finite size correction should be $O(1/L)$ (see section 5.2), our simulation results are consistent with the predictions.

Appendix J. Derivation of (63)

In this appendix, we calculate the joint probability $P_2(\sigma_1, \sigma_2)$ that two genotypes σ_1, σ_2 are both local fitness maxima for FGM with $n = 1$. Let us consider two genotypes with the following sequences,

$$\begin{aligned} \sigma_1 &= \{\overbrace{1, 1, \dots, 1}^{u_3}, \overbrace{1, 1, \dots, 1}^{u_2}, \overbrace{0, 0, \dots, 0}^{u_1}, \overbrace{0, 0, \dots, 0}^{u_0}\}, \\ \sigma_2 &= \{\overbrace{1, 1, \dots, 1}^{u_3}, \overbrace{0, 0, \dots, 0}^{u_2}, \overbrace{1, 1, \dots, 1}^{u_1}, \overbrace{0, 0, \dots, 0}^{u_0}\}, \end{aligned} \quad (\text{J.1})$$

where the u_i 's have the same meaning as in (60). We denote the random phenotype variables associated with the sites in the regions of size u_0 , u_1 , u_2 , and u_3 by ξ_i , ζ_j , η_k , and ν_l , respectively. Accordingly, the phenotypes x and y corresponding to the genotypes σ_1 and σ_2 are

$$x = \sum_{k=1}^{u_2} \eta_k + \sum_{l=1}^{u_3} \nu_l, \quad y = \sum_{j=1}^{u_1} \zeta_j + \sum_{l=1}^{u_3} \nu_l. \quad (\text{J.2})$$

Defining

$$\mathcal{D}(w, v) = \{z \in \mathbb{R} \mid |z - w| > |w| \ \& \ |z - v| > |v|\}, \quad (\text{J.3})$$

$P_2(\sigma_1, \sigma_2)$ can be formally written as

$$\begin{aligned} P_2 &= \int dx dy \prod_{i=1}^{u_0} \int_{\mathcal{D}(-x, -y)} d\xi_i p(\xi_i) \prod_{j=1}^{u_1} \int_{\mathcal{D}(-x, y)} d\zeta_j p(\zeta_j) \prod_{k=1}^{u_2} \int_{\mathcal{D}(x, -y)} d\eta_k p(\eta_k) \\ &\quad \prod_{l=1}^{u_3} \int_{\mathcal{D}(x, y)} d\nu_l p(\nu_l) \delta\left(x - \sum_{k=1}^{u_2} \eta_k - \sum_{l=1}^{u_3} \nu_l\right) \delta\left(y - \sum_{j=1}^{u_1} \zeta_j - \sum_{l=1}^{u_3} \nu_l\right). \end{aligned} \quad (\text{J.4})$$

Using the integral representation of the delta function, we get

$$P_2 = \int \frac{dk_x dk_y dx dy}{(2\pi)^2} \exp(ik_x x + ik_y y) I(-x, -y, 0)^{u_0} I(-x, y, k_y)^{u_1} I(x, -y, k_x)^{u_2} I(x, y, k_x + k_y)^{u_3}, \quad (\text{J.5})$$

where

$$I(x, y, k) = \int_{\mathcal{D}(x,y)} dz p(z) \exp(-ikz). \quad (\text{J.6})$$

As discussed in Appendix B, the dominant contribution for large u_i comes from the region of small x, y, k_x, k_y . Expanding the integrand for small x, y , and k , we have

$$I(x, y, k) = \exp\left(-\frac{k^2}{2}\right) - p(0)\epsilon(x, y) [1 + \mathcal{O}(k)], \quad (\text{J.7})$$

where

$$\begin{aligned} \epsilon(x, y) &= \int_{\mathbb{R} \setminus \mathcal{D}(x,y)} \frac{p(z)}{p(0)} dz \approx \int_{\mathbb{R} \setminus \mathcal{D}(x,y)} dz \\ &= \max(|x| - x, |y| - y) + \max(x + |x|, y + |y|). \end{aligned} \quad (\text{J.8})$$

Using these results, the leading contribution to (J.5) becomes

$$\begin{aligned} P_2 &\approx \int \frac{dk_x dk_y}{2\pi} \exp\left[-\frac{u_3}{2}(k_x + k_y)^2 - \frac{u_1}{2}k_x^2 - \frac{u_2}{2}k_y^2\right] \\ &\quad \int dx dy \exp[-u_0\epsilon(-x, -y) - u_1\epsilon(-x, y) - u_2\epsilon(x, -y) - u_3\epsilon(x, y)] \\ &= \frac{3}{(u_0 + 2u_1 + 2u_2 + u_3)(2u_0 + u_1 + u_2 + 2u_3)\sqrt{u_1u_2 + u_1u_3 + u_2u_3}}. \end{aligned} \quad (\text{J.9})$$

Calculating P_1 can be done in a similar manner:

$$P_1(\sigma_1) = \int \frac{dk dx}{2\pi} \exp(ikx) I_1(-x, 0)^{L-d_1} I_2(x, k)^{d_1}, \quad (\text{J.10})$$

where $d_1 = u_2 + u_3$ and

$$I_1(x, k) = \int_{\mathcal{D}[x]} dz p(z) \exp(-ikz) = \exp\left(-\frac{k^2}{2}\right) - 2p(0)|x| [1 + \mathcal{O}(k)]. \quad (\text{J.11})$$

For large d_1 and $L - d_1$, we obtain

$$P_1 = \frac{1}{L\sqrt{d_1}}. \quad (\text{J.12})$$

Using $u_0 + u_1 + u_2 + u_3 = L$, we arrive at (63).

References

- [1] H. Allen Orr. The genetic theory of adaptation: A brief history. *Nat. Rev. Genet.*, 6:119–127, 2005.

- [2] J. A. G. M. de Visser and Joachim Krug. Empirical fitness landscapes and the predictability of evolution. *Nat. Rev. Genet.*, 15:480–490, 2014.
- [3] I. Fragata, A. Blanckaert, M. A. Dias Louro, D. A. Liberles, and C. Bank. Evolution in the light of fitness landscape theory. *Trends Ecol. Evol.*, 34:69–82, 2019.
- [4] S. Wright. Evolution in Mendelian populations. *Genetics*, 16:97–159, 1931.
- [5] Ivan G. Szendro, Martijn F. Schenk, Jasper Franke, Joachim Krug, and J. Arjan G.M. de Visser. Quantitative analyses of empirical fitness landscapes. *J. Stat. Mech.:Theory Exp.*, page P01005, 2013.
- [6] John H. Gillespie. Molecular evolution over the mutational landscape. *Evolution*, 38:1116–1129, 1984.
- [7] H. Allen Orr. The population genetics of adaptation: the adaptation of DNA sequences. *Evolution*, 56:1317–1330, 2002.
- [8] G. Sella and A. E. Hirsh. The application of statistical physics to evolutionary biology. *Proc. Nat. Acad. Sci. USA*, 102:9541–9546, 2005.
- [9] P. F. Stadler and R. Happel. Random field models for fitness landscapes. *J. Math. Biol.*, 38:435–478, 1999.
- [10] S. Hwang, B. Schmiegelt, L. Ferretti, and J. Krug. Universality classes of interaction structures for NK fitness landscapes. *J. Stat. Phys.*, 172:226–278, 2018.
- [11] J. Domingo, P. Baeza-Centurion, and B. Lehner. The causes and consequences of genetic interactions (epistasis). *Ann. Rev. Genom. Hum. Genet.*, 20:17.1–17.28, 2019.
- [12] S. Manrubia, J.A. Cuesta, J. Aguirre, S.E. Ahnert, L. Altenberg, A.V. Cano, P. Catalán, R. Diaz-Uriarte, S.F. Elena, J.A. García-Martín, P. Hogeweg, B.S. Khatri, J. Krug, A.A. Louis, N.S. Martin, J.L. Payne, M.J. Tarnowski, and M. Weiß. From genotypes to organisms: State-of-the-art and perspectives of a cornerstone in evolutionary dynamics. *Preprint*, arXiv:2002.00363, 2020.
- [13] R. A. Fisher. *The Genetical Theory of Natural Selection*. Clarendon Press, Oxford, 1930.
- [14] Guillaume Martin, Santiago F. Elena, and Thomas Lenormand. Distributions of epistasis in microbes fit predictions from a fitness landscape model. *Nat. Gen.*, 39:555–560, 2007.
- [15] Pierre-Alexis Gros, Hervé Le Nagard, and Olivier Tenaillon. The evolution of epistasis and its links with genetic robustness, complexity and drift in a phenotypic model of adaptation. *Genetics*, 182:277–293, 2009.
- [16] Guillaume Martin. Fisher's geometric model emerges as a property of complex integrated phenotypic networks. *Genetics*, 197:237–255, 2014.
- [17] Francois Blanquart, Guillaume Achaz, Thomas Bataillon, and Olivier Tenaillon. Properties of selected mutations and genotypic landscapes under Fisher's geometric model. *Evolution*, 68:3537–3554, 2014.
- [18] Olivier Tenaillon. The utility of Fisher's geometric model in evolutionary genetics. *Annu. Rev. Ecol. Evol. Syst.*, 45:179–201, 2014.
- [19] Sungmin Hwang, Su-Chan Park, and Joachim Krug. Genotypic complexity of Fisher's geometric model. *Genetics*, 206(2):10491079, 2017.
- [20] Sijmen Schoustra, Sungmin Hwang, Joachim Krug, and J. Arjan G.M. de Visser. Diminishing-returns epistasis among random beneficial mutations in a multicellular fungus. *Proc. R. Soc. Lond. Ser. B*, 283:20161376, 2016.
- [21] J. J. Hopfield. Neural networks and physical systems with emergent collective computational abilities. *Proc. Nat. Acad. Sci. USA*, 79(8):2554–2558, April 1982.
- [22] Daniel J. Amit. *Modeling brain function: The world of attractor neural networks*. Cambridge University Press, Cambridge, UK, 1989.
- [23] J. A. Hertz, A. Krogh, and R. G. Palmer. *Introduction to the theory of neural computation*. Taylor-Francis, Boca Raton, 1991.
- [24] Kazuo Nokura. Spin glass states of the anti-Hopfield model. *J. Phys. A*, 31:7447–7459, 1998.
- [25] R. Cherrier, D. S. Dean, and A. Lefèvre. The number of metastable states in the generalized

- random orthogonal model. *J. Phys. A: Math. Gen.*, 36(14):3935, 2003.
- [26] D. Challet and Y. C. Zhang. Emergence of cooperation and organization in an evolutionary game. *Physica A*, 246(3):407–418, December 1997.
- [27] Matteo Marsili, Damien Challet, and Riccardo Zecchina. Exact solution of a modified El Farol's bar problem: Efficiency and the role of market impact. *Physica A*, 280(34):522–553, June 2000.
- [28] Damien Challet, Matteo Marsili, and Riccardo Zecchina. Statistical Mechanics of Systems with Heterogeneous Agents: Minority Games. *Phys. Rev. Lett.*, 84(8):1824–1827, February 2000.
- [29] Anirban Chakraborti, Damien Challet, Arnab Chatterjee, Matteo Marsili, Yi-Cheng Zhang, and Bikas K. Chakrabarti. Statistical mechanics of competitive resource allocation using agent-based models. *Physics Reports*, 552:1 – 25, 2015.
- [30] F. F. Ferreira and J. F. Fontanari. Probabilistic analysis of the number partitioning problem. *J. Phys. A*, 31:3417–3428, 1998.
- [31] S. Mertens. Random costs in combinatorial optimization. *Phys. Rev. Lett.*, 84:1347–1350, 2000.
- [32] F Tanaka and S F Edwards. Analytic theory of the ground state properties of a spin glass. I. Ising spin glass. *J. Phys. F: Met. Phys.*, 10(12):2769, 1980.
- [33] A J Bray and M A Moore. Metastable states in spin glasses. *J. Phys. C: Solid State Phys.*, 13(19):L469–L476, 1980.
- [34] A. J. Bray and M. A. Moore. Metastable states in spin glasses with short-ranged interactions. *J. Phys. C: Solid State Phys.*, 14(9):1313, 1981.
- [35] E. Gardner. Structure of metastable states in the Hopfield model. *J. Phys. A: Math. Gen.*, 19(16):L1047, 1986.
- [36] A. Treves and D. J. Amit. Metastable states in asymmetrically diluted Hopfield networks. *J. Phys. A: Math. Gen.*, 21(14):3155, 1988.
- [37] Manoranjan P. Singh, Zhang Chengxiang, and Chandan Dasgupta. Fixed points in a Hopfield model with random asymmetric interactions. *Phys. Rev. E*, 52(5):5261–5272, November 1995.
- [38] Francois Blanquart and Thomas Bataillon. Epistasis and the structure of fitness landscapes: are experimental fitness landscapes compatible with Fisher's geometric model? *Genetics*, 203:847–862, 2016.
- [39] Daniel M. Weinreich and Jennifer L. Knies. Fisher's geometric model of adaptation meets the functional synthesis: Data on pairwise epistasis for fitness yields insights into the shape and size of phenotype space. *Evolution*, 67:2957–2972, 2013.
- [40] A Erdélyi, editor. *Higher Transcendental Functions*, volume 1. McGraw-Hill, New York, 1955.
- [41] Stefan Nowak and Joachim Krug. Analysis of adaptive walks on NK fitness landscapes with different interaction schemes. *J. Stat. Mech.:Theory Exp.*, 2015:P06014, 2015.
- [42] J. F. C. Kingman. A simple model for the balance between selection and mutation. *J. Appl. Prob.*, 15:1–12, 1978.
- [43] S. Kauffman and S. Levin. Towards a general theory of adaptive walks on rugged landscapes. *J. Theor. Biol.*, 128:11–45, 1987.
- [44] B. Derrida. Random-energy model - an exactly solvable model of disordered systems. *Phys. Rev. B*, 24(5):2613–2626, 1981.
- [45] C. A. Macken and A. S. Perelson. Protein evolution on rugged landscapes. *Proc. Nat. Acad. Sci. USA*, 86:6191–6195, 1989.
- [46] P. Baldi and Y. Rinott. Asymptotic normality of some graph-related statistics. *J. Appl. Prob.*, 26:171–175, 1989.
- [47] A. S. Perelson and C. A. Macken. Protein evolution on partially correlated landscapes. *Proc. Nat. Acad. Sci. USA*, 92:9657–9661, 1995.
- [48] B. Schmiegelt and J. Krug. Evolutionary accessibility of modular fitness landscapes. *J. Stat. Phys.*, 154:334–355, 2014.
- [49] S Hwang, D. S. Dean, and J Krug. (unpublished).
- [50] Marcin Zagorski, Zdzislaw Burda, and Bartłomiej Waclaw. Beyond the hypercube: Evolutionary accessibility of fitness landscapes with realistic mutational networks. *PLoS Comp. Biol.*,

12:e1005218, 2016.

- [51] B. Schmiegelt and J. Krug. Accessibility percolation on cartesian power graphs. *Preprint*, arXiv:1912.07925, 2020.
- [52] S Hwang and J Krug. (unpublished).
- [53] Victoria O. Pokusaeva, Dinara R. Usmanova, Ekaterina V. Putintseva, Lorena Espinar, Karen S. Sarkisyan, Alexander S. Mishin, Natalya S. Bogatyreva, Dmitry N. Ivankov, Arseniy V. Akopyan, Sergey Ya. Avvakumov, Inna S. Povolotskaya, Guillaume J. Fillion, Lucas B. Carey, and Fyodor A. Kondrashov. An experimental assay of the interactions of amino acids from orthologous sequences shaping a complex fitness landscape. *PLoS Genet.*, 15:e1008079, 2019.